




## Article

# Pectin Nanoparticle-Loaded Soft Coral *Nephthea* sp. Extract as *In Situ* Gel Enhances Chronic Wound Healing: *In Vitro*, *In Vivo*, and *In Silico* Studies

Nevine H. Hassan <sup>1</sup>, Seham S. El-Hawary <sup>2</sup>, Mahmoud Emam <sup>3</sup>, Mohamed A. Rabeh <sup>4</sup>, Mohamed A. Tantawy <sup>5,6,7</sup>, Mohamed Seif <sup>8</sup>, Radwa M. A. Abd-Elal <sup>9,\*</sup>, Gerhard Bringmann <sup>10</sup>, Usama Ramadan Abdelmohsen <sup>11,12,\*</sup> and Nabil M. Selim <sup>2,\*</sup>

- <sup>1</sup> Pharmacognosy Department, Faculty of Pharmacy, Modern University for Technology and Information, Cairo 11571, Egypt; nevine.hossam@pharm.mti.edu.eg
- <sup>2</sup> Pharmacognosy Department, Faculty of Pharmacy, Cairo University, Giza 11562, Egypt; seham.elhawary@pharma.cu.edu.eg
- <sup>3</sup> Phytochemistry and Plant Systematics Department, National Research Centre, Dokki, Cairo 12622, Egypt; mahmouDEMAMHEGazy2020@gmail.com
- <sup>4</sup> Pharmacognosy Department, College of Pharmacy, King Khalid University, Abha 62514, Saudi Arabia; mrabeh@kku.edu.sa
- <sup>5</sup> Hormones Department, Medical Research and Clinical Studies Institute, National Research Centre, Dokki, Cairo 12622, Egypt; mohamed\_tantawy@daad-alumni.de
- <sup>6</sup> Stem Cells Lab Center of Excellence for Advanced Sciences, National Research Centre, Dokki, Cairo 12622, Egypt
- <sup>7</sup> Center of Orthopaedics Research, and Translation Science (CORTS), Department of Orthopaedics and Rehabilitation, The Pennsylvania State University College of Medicine, State College, PA 16801, USA
- <sup>8</sup> Toxicology and Food Contaminants Department, Food Industries and Nutrition Research Institute, National Research Centre, Giza 12622, Egypt; seif.eg@gmail.com
- <sup>9</sup> Pharmaceutics and Drug Manufacturing Department, Faculty of Pharmacy, Modern University for Technology and Information, Cairo 11571, Egypt
- <sup>10</sup> Institute of Organic Chemistry, University of Würzburg, Am Hubland, 97074 Würzburg, Germany; bringman@chemie.uni-wuerzburg.de
- <sup>11</sup> Pharmacognosy Department, Faculty of Pharmacy, Minia University, Minia 61519, Egypt
- <sup>12</sup> Pharmacognosy Department, Faculty of Pharmacy, Deraya University, New Minia 61111, Egypt
- \* Correspondence: radwa.mahrous@pharm.mti.edu.eg (R.M.A.A.-E.); usama.ramadan@mu.edu.eg (U.R.A.); nabil.selim@pharma.cu.edu.eg (N.M.S.); Tel.: +2-20311120 (R.M.A.A.-E.); +2-086-2369075 (U.R.A.); +2-32628426 (N.M.S.)



**Citation:** Hassan, N.H.; El-Hawary, S.S.; Emam, M.; Rabeh, M.A.; Tantawy, M.A.; Seif, M.; Abd-Elal, R.M.A.; Bringmann, G.; Abdelmohsen, U.R.; Selim, N.M. Pectin Nanoparticle-Loaded Soft Coral *Nephthea* sp. Extract as *In Situ* Gel Enhances Chronic Wound Healing: *In Vitro*, *In Vivo*, and *In Silico* Studies. *Pharmaceuticals* **2023**, *16*, 957. <https://doi.org/10.3390/ph16070957>

Academic Editor: Dimitris Tsiourvas

Received: 31 May 2023  
Revised: 25 June 2023  
Accepted: 30 June 2023  
Published: 3 July 2023



**Copyright:** © 2023 by the authors. Licensee MDPI, Basel, Switzerland. This article is an open access article distributed under the terms and conditions of the Creative Commons Attribution (CC BY) license (<https://creativecommons.org/licenses/by/4.0/>).

**Abstract:** This study shed light for the first time on the *in vivo* diabetic wound healing potential activity of natural marine soft coral polymeric nanoparticle *in situ* gel using an excision wound model. A *Nephthea* sp. methanol–methylene chloride extract loaded with pectin nanoparticles (LPNs) was created. For the preparation of *in situ* gel, ion-gelation techniques, the entrapment efficiency, the particle size, the polydispersity index, the zeta potential, the *in-vitro* drug release, and a transmission electron microscope were used and the best formula was selected. Using (UPLC-Q/TOF-MS), 27 secondary metabolites responsible for extract biological activity were identified. Isolation and identification of arachidic acid, oleic acid, nervonic acid, and bis-(2-ethylhexyl)-phthalate (DEHP) of *Nephthea* sp. was firstly reported here using NMR and mass spectral analyses. Moreover, LPN *in situ* gel has the best effects on regulating the proinflammatory cytokines (NF- $\kappa$ B, TNF- $\alpha$ , IL-6, and IL-1 $\beta$ ) that were detected on days 7 and 15. The results were confirmed with an *in vitro* enzymatic inhibitory effect of the extract against glycogen synthase kinase (GSK-3) and matrix metalloproteinase-1 (MMP-1), with IC<sub>50</sub> values of  $0.178 \pm 0.009$  and  $0.258 \pm 0.011$   $\mu$ g/mL, respectively. The molecular docking study showed a free binding energy of  $-9.6$  kcal/mol for chabrolosteroid E, with the highest binding affinity for the enzyme (GSK-3), while isogosterone B had  $-7.8$  kcal/mol for the enzyme (MMP-1). A pharmacokinetics study for chabrolohydroxybenzoquinone F and isogosterone B was performed, and it predicted the mode of action of wound healing activity.

**Keywords:** ADME; *in situ* gel; molecular docking; *Nephthea* sp.; pectin nanoparticles; wound healing

## 1. Introduction

Skin wounds are considered as a global health issue due to their ability to kill more than 5 million people each year and contribute significantly to disease burden mainly to people of a low socioeconomic status [1]. Wounds are classified as physical, thermal, or chemical injuries that create an opening in the integrity of the skin or change the anatomical integrity of living tissues [2]. The plurality of chronic wounds are ulcers produced by diabetes mellitus, pressure, ischemia, and excessive obesity [3]. Wound healing medicines must be biocompatible, non-toxic, hypoallergenic, able to maintain a moist environment, protect the wound from germs, and encapsulate wound exudates [4]; this established the urgent need for the development of innovative safe therapies in this field [5].

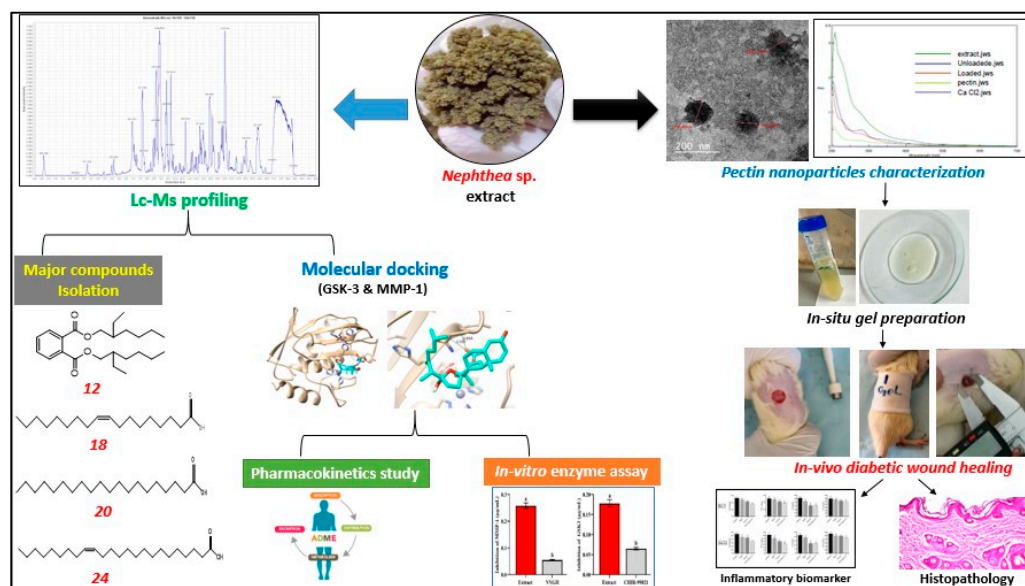
Nanoscience is one of the most recent sciences to pique the interest of scientists [6]. This is a brand new field that involves the creation and application of nanoscale-size materials to a variety of applications, and they are especially hygienic, non-toxic, and ecologically friendly [7]. Natural resources have the potential to be used to create nanoparticles that are bioactive and compatible with biological systems but this potential has not been completely examined [8,9].

Pectin is a naturally anionic water-soluble polysaccharide polymer, derived from the cell walls of certain citrus plants [10]. Due to its cross-linked properties, non-toxicity, bio-compatibility, mucoadhesion properties, water absorption capacity, moisture retention, and anti-inflammatory activity [11], pectin is an attractive choice to form polymeric pectin nanoparticles to encapsulate both hydrophilic and lipophilic compounds [12].

Smart polymers have been used to create stimuli-responsive *in situ* gels; these polymers tend to change their consistency in response to physiological changes. The *in situ* gels created with these polymers initially take the form of a solution and after being administered to the skin, go through a phase transition (from sol to gel) in response to heat stimulation, pH changes, or ionic concentration [13].

The genus *Nephthea* has been discovered to produce secondary metabolites like sesquiterpenes, fatty acids, terpenes, and steroids [14]. Additionally, a review on the scientific literature on the biological efficacy of the octocoral *Nephthea* sp. revealed that it can act as an inhibitor of dermatophytes [15] as well as an antiviral [16], antibiofilm [17], anti-COVID-19 [18], and gastroprotective agent [19].

To the best of our knowledge, the wound healing potential activity of the soft coral *Nephthea* sp. has not been previously evaluated. Therefore, the novelty of our study is the investigation of the chronic wound healing stimulation activity of the pharmaceutical preparation of polymer nanoparticle-loaded *Nephthea* sp., which was obtained from the Red Sea region. The pectin nanoparticle-loaded *Nephthea* sp. extract prepared with an ion-gelation technique at 0.5% *w/v* of pectin with CaCl<sub>2</sub> as a cross-linker in a different ratio was elucidated with *in vitro* studies, including the entrapment efficiency, particle size, polydispersity index, zeta potential, *in vitro* release study, and morphological study with a transmission electron microscope, to select the optimized formulation, and it was incorporated as an *in situ* gel dosage form for transdermal drug delivery in diabetic-wound rats. Additionally, the metabolic profile of the *Nephthea* sp. extract was examined using the UPLC-Q/TOF-MS technique, then the major identified components were isolated. Additionally, NF- $\kappa$ B and pro-inflammatory cytokines (TNF- $\alpha$ , IL-6, and IL-1 $\beta$ ) were measured for the different treatments in the middle and at the end of the experiment. Furthermore, the inhibitory action of the extract against GSK-3 and MMP-1 enzymes was tested to confirm the mechanism of action toward wound healing activity. Finally, an *in silico* study of the identified metabolites against GSK-3 and MMP-1 enzymes was assembled, followed by pharmacokinetics and an ADME profile of the high-binding components (Scheme 1).



**Scheme 1.** The comprehensive overview of the steps for the extraction of a soft coral sample, characterization of pectin nanoparticles, *in situ* gel, *in vivo* diabetic wound healing assay, histopathological examination of the skin, inflammatory biomarker, metabolomic analysis, isolated metabolites, docking study, ADME activity, and *in vitro* enzymatic inhibition assay.

## 2. Results and Discussion

### 2.1. Preparation and Characterization of SCN-LPN

The ion-gelation method was successful in loading SCN within the formed pectin nanoparticles with different ratios of  $\text{CaCl}_2$  as a cross-linker. This might be related to the positively charged  $\text{CaCl}_2$ , which was successfully cross-linked with the negatively charged pectin molecules by an intermolecular cross-link, which is formed by electrostatic complexation interaction [20].

The % E.E. indicates how the formed particles can load sufficient quantities of the drug. As shown in Table 1, all the formed SCN-LPN formulations had an E.E. value higher than 90%, and increasing the pectin-to- $\text{CaCl}_2$  ratio from 1:1 to 1:3 had a non-significant difference on the E.E. value ( $p > 0.05$ ). This could be related to the hydrophobic nature of SCN, which contains sesquiterpenes, diterpenes, and sterols, so it can easily entrap into polymeric nanoparticles during a sudden electron complexation between negatively charged pectin molecules and  $\text{CaCl}_2$ . Thereby, a limited drug leakage from the formed polymeric nanoparticles occurred.

The formed SCN-LPN had acceptable PS, ranging between  $241.5 \pm 17.5$  and  $288.2 \pm 25.66$  nm with low PDI values ranging from  $0.290 \pm 0.22$  to  $0.523 \pm 0.12$ , which indicated the homogeneity of the formed SCN-LPN formulations. In addition to this, it was observed that raising the pectin-to- $\text{CaCl}_2$  ratios from 1:1 to 1:2 was associated with a significant increase in the particle size of the formed SCN-LPN ( $p < 0.05$ ). This could be related to an enhanced number of  $\text{CaCl}_2$  molecules that interacted electrostatically with the pectin chains, resulting in the formation of a large SCN-LPN size [21]. However, with any further increase in the pectin-to- $\text{CaCl}_2$  ratio above 1:2, a significant decrease in PS was observed. There was a direct relation between the amount of SCN loaded within the formed nanoparticles and their particle size, as shown in Table 1.

The ZP value is a crucial parameter of nanoparticles, in addition to PS, since it can show the stability of the nanoparticle formulations [22,23]. Higher absolute ZP values can strengthen the stability of the system related to a strong electrostatic repulsion between the particles that also prevent the agglomeration between them, or it could be related to the ionization of carboxyl groups of pectin [21]. All the SCN-LPN formulations had a negative charge of ZP ranging between  $-5.34 \pm 1.20$  and  $-16.6 \pm 2.4$  mV due to the ionization

of the carboxyl group of pectin. Increasing the pectin-to- $\text{CaCl}_2$  ratio was accomplished by decreasing the ZP value of the prepared SCN-LPN ( $p < 0.05$ ). This could be explained with a strong neutralization of the negative charges of the free carboxyl groups of pectin with divalently charged  $\text{CaCl}_2$  as a cross-linker [21,24]. From the previous results, the selected formulation for further studying was SCN-LPN2 with a % E.E. of  $98.55 \pm 2.20$ , PS of  $288.2 \pm 25.66$ , PDI of  $0.381 \pm 0.12$ , and ZP of  $-16.6 \pm 2.4$ , as shown in Figure 1.

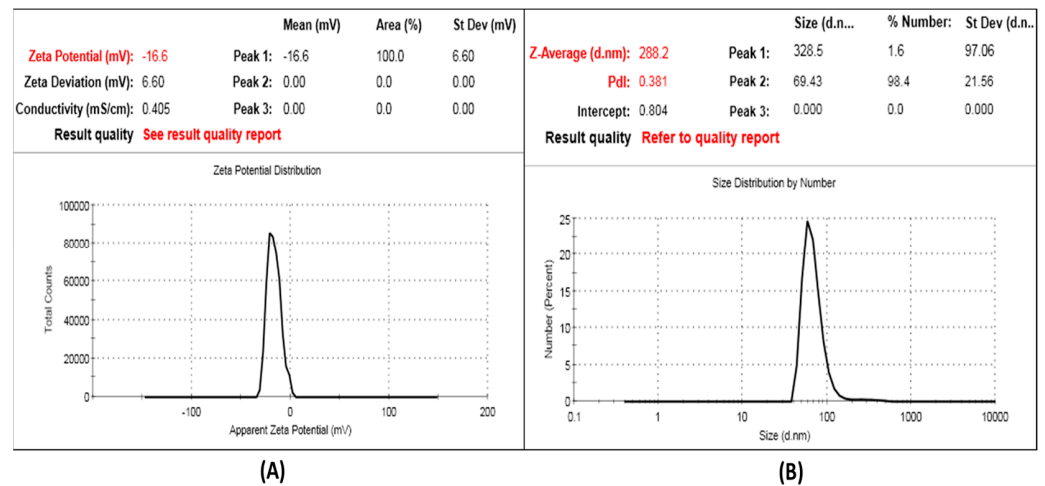


**Figure 1.** (A) Electrophoretic mobility and (B) size distribution images of the selected SCN-LPN2 formulation.

#### 2.1.1. HRTEM Characterization of the Selected SCN-LPN

The morphology of the selected formula (SCN-LPN2) was evaluated with an HRTEM analysis and is depicted in Figure 2. It showed that the prepared nanoparticles were uniform and spherical in shape and no agglomeration was observed. The mean particle size was obtained with the HRTEM analysis of nanosized particles; this followed the results obtained with Zeta-sizer equipment. In addition, selected area electron diffraction (SAED) confirmed that the prepared formulation had an amorphous property with no SCN crystals being observed.

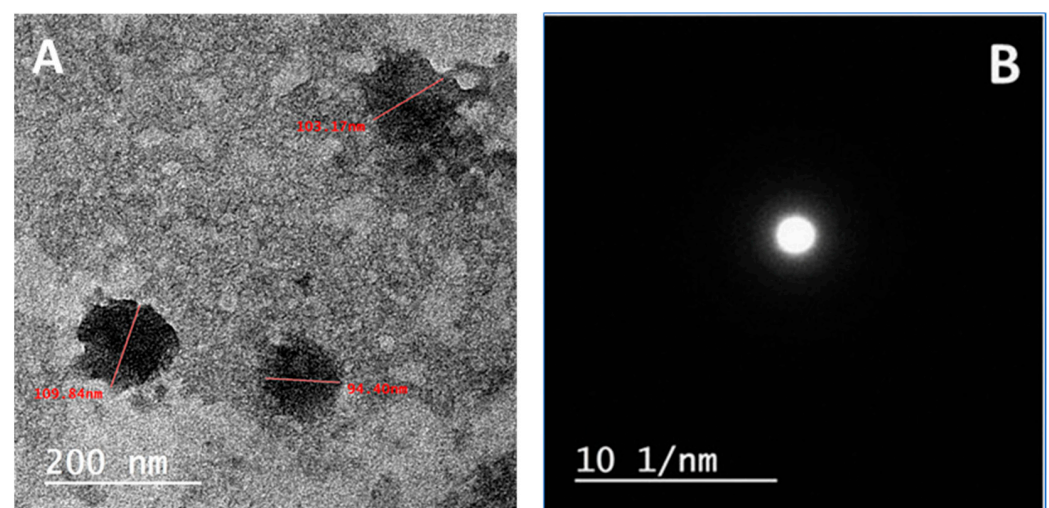


**Figure 2.** (A) The HRTEM image for the shape and size. (B) The selected area electron diffraction (SAED) image of the selected SCN loaded with nanoparticles (SCN-LPN2).

#### 2.1.2. UV-Visible and FTIR Characterization of the Selected SCN-LPN Formulation

The chemical structure of the selected SCN-LPN formulation was evaluated with UV-Vis and FTIR spectroscopy. The formation of SCN-LPN2 was monitored by measuring



the UV-Vis spectrum of the reaction medium in the wavelength range from 200 to 600 nm. Figure 3 illustrates the UV-Vis spectra of the *Nephthea* sp. extract, showing an absorption maximum peak at 415 nm, while the unloaded formula exhibited a  $\lambda_{\max}$  band at 350 nm. Upon the interaction between both the mixtures “unloaded and the extract” being performed, the observed bands disappeared, indicating that the interaction between the two mixtures was achieved and the “loaded” SCN-LPN2 formula was prepared.

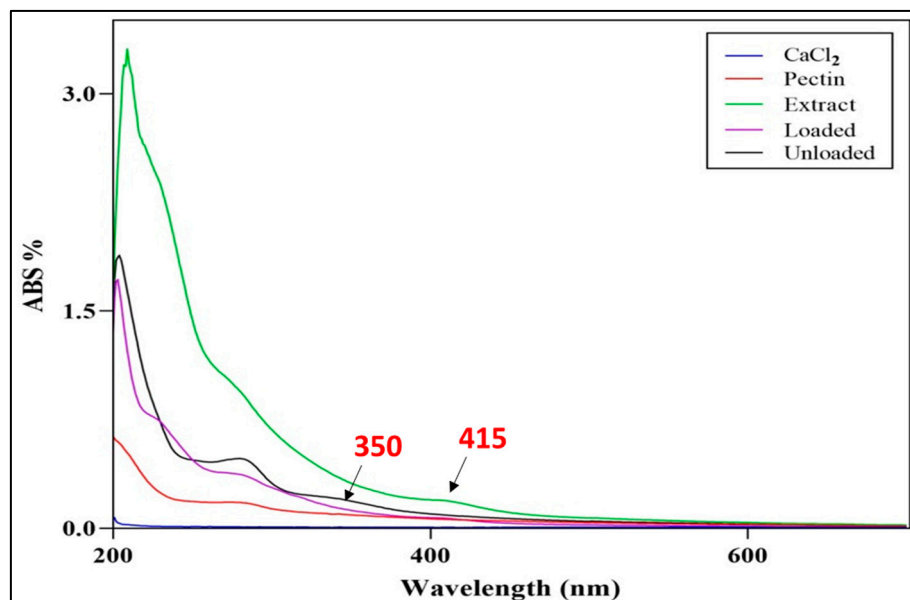


**Figure 3.** The  $\lambda_{\max}$  bands of SCN-LPN2 (loaded), unloaded SCN-LPN2, pectin, CaCl<sub>2</sub>, and the *Nephthea* sp. extract were recorded with UV-vis spectra.

Using FTIR spectroscopy, the chemical structure of the selected loaded formulation was investigated and compared with the unloaded formulation, extract, CaCl<sub>2</sub>, and pectin structures; see Figure 4. The peaks at 3351, 1716, and 1644 cm<sup>-1</sup> in the pectin, extract, and unloaded samples were observed, indicating the presence of OH and C=O functional groups, while after adding the mixture of the extract and unloaded formula, these observed peaks were shifted and shortened, which indicated that the interaction was taking place. These spectroscopic findings supported the creation of the SCN-LPN.

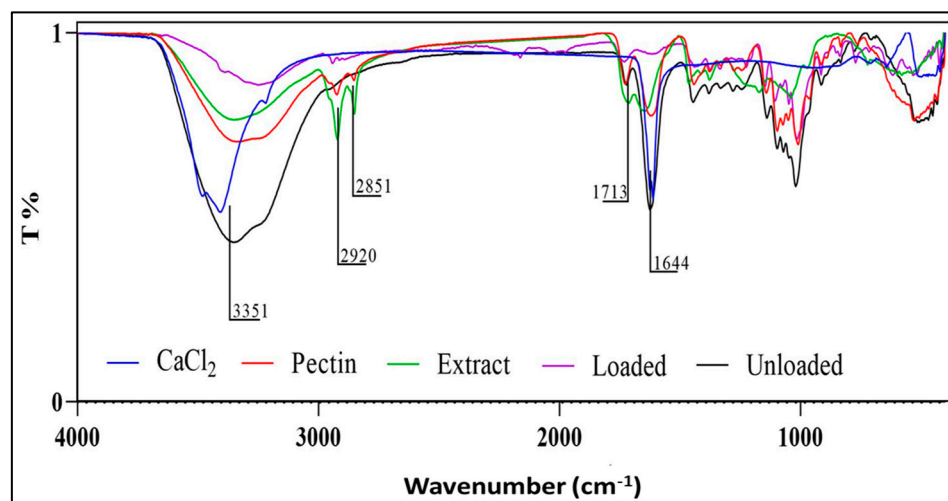


**Figure 4.** FTIR spectra of the pectin, unloaded formula, and CaCl<sub>2</sub> as compared with that of the SCN-LPN2-stabilized pectin nanoparticles (loaded formula).

### 2.1.3. Characterization of SCN-LPN-ISG

SCN-LPN2-ISG appeared as a homogeneous, yellowish clear system related to the color of SCN at a suitable pH value ( $6.5 \pm 0.5$ ) for skin application without any irritation. The drug content value was  $99.43 \pm 1.1$ , indicating the uniformity of distribution during the preparation of *in situ* gel. The *sol-gel* transition temperature of the prepared SCN-LPN2-ISG was  $32.20 \text{ }^\circ\text{C} \pm 0.65$ , ideal for skin application, and this could be due to a suitable combination ratio between PF<sup>®</sup>127 and PF<sup>®</sup>68, because PF<sup>®</sup>68 could decrease the total polymer content and improve gelling properties of PF<sup>®</sup>127.

The viscosities of the SCN-LPN2-ISG freshly prepared before gelling ( $25 \text{ }^\circ\text{C}$ ) at 1 rpm and 10 rpm were found to be  $82.55 \pm 11.70$  and  $40.66 \pm 6.88$ , respectively. The viscosities were raised to  $19,234.22 \pm 210.24$  and  $2805.55 \pm 177.63$ , respectively, as a response to the temperature ( $37 \text{ }^\circ\text{C}$ ), meaning that the viscosity of the prepared SCN-LPN2-ISG was drastically increased when raising the temperature from  $25 \text{ }^\circ\text{C}$  to  $37 \text{ }^\circ\text{C}$ , where gelling will occur, owing to the thermo-sensitive properties of the prepared ISG.

The cumulative amount of SCN (%) released from the SCN suspension, selected SCN-LPN2, and SCN-LPN2-ISG at different time intervals is graphically illustrated in Figure 5. Almost 90% of the SCN amount was released from the SCN suspension in the first 2 h. However, the selected SCN-LPN2 and SCN-LPN2-ISG released around 30% of the loaded drug in the first 2 h and succeeded in retarding the remaining loaded drug for 8 h in comparison with the SCN suspension. This could be related to the nanoparticle matrix, which acts as a barrier to drug release toward the dissolution medium [25].

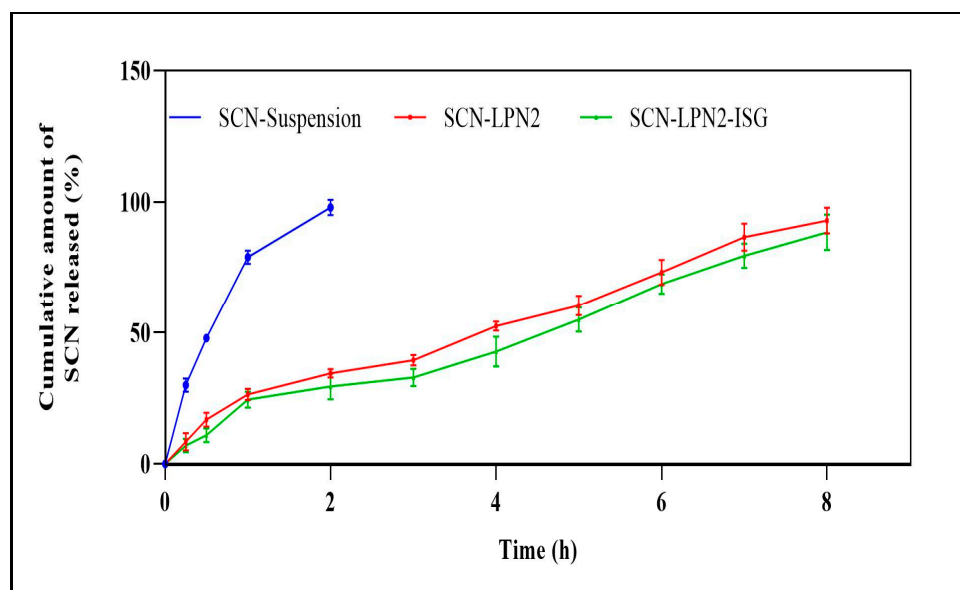


**Figure 5.** The *in vitro* release profile of the SCN suspension, selected SCN-LPN2, and SCN-LPN2-ISG. Error bars represent SD.

### 2.2. Metabolomic Profiling Study

The UPLC-Q/TOF-MS profile of the *Nephthea* sp. extract is shown in Figures 6 and S1, and Table 1. Table 1 provides the retention times, identities, observed molecular weights, and ionization modes for the recognized metabolites. Using macros, MZmine-based methods, and internet databases (databases DNP and MarinLit), 27 metabolites were identified, the majority of which were compared with previously reported published data from the Nephtheidae family and classified as described in the following reference: [16].

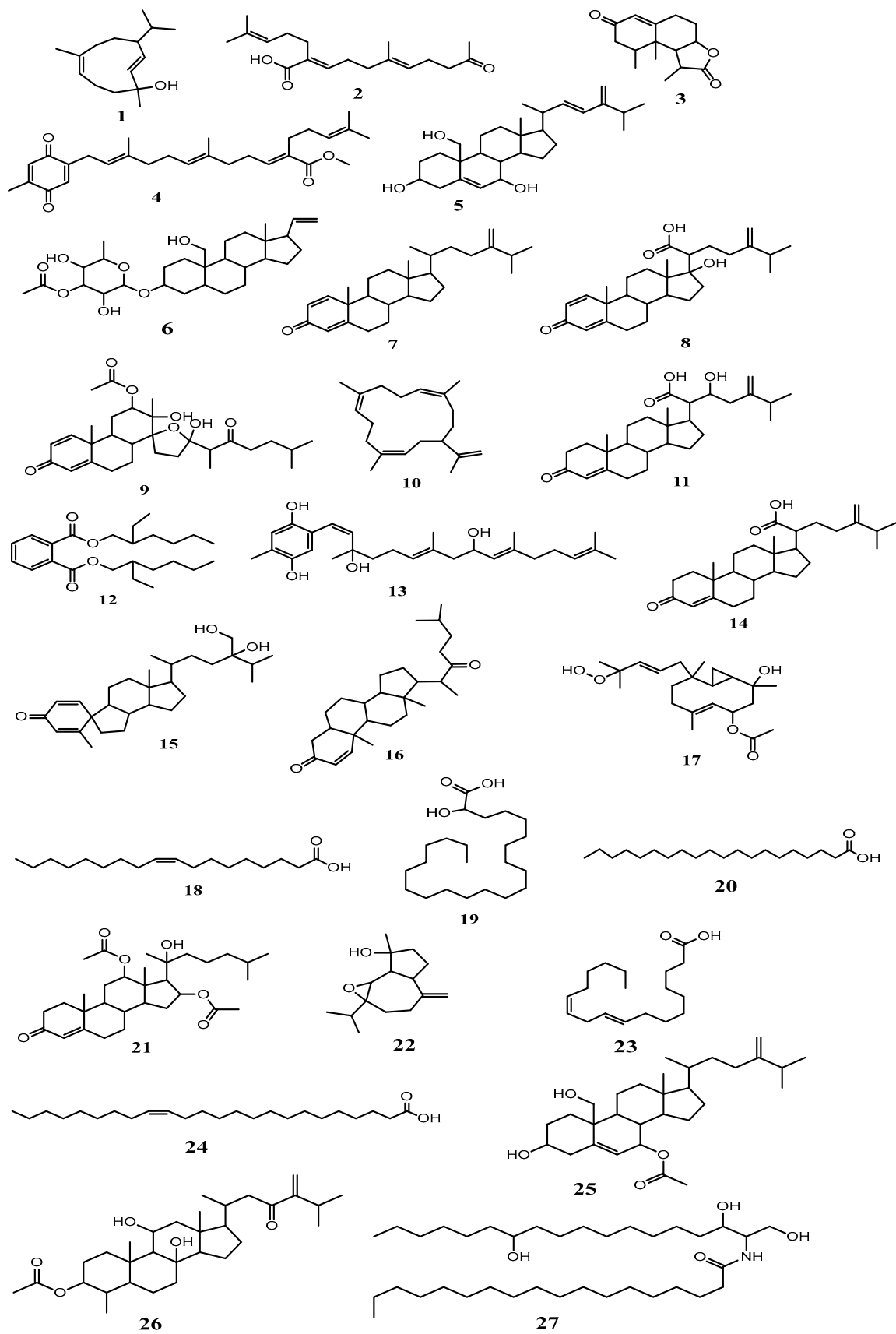


**Figure 6.** The proposed chemical structures of the compounds identified and dereplicated from the *Nephthea* sp.

Sterols possessing the mass ions of  $m/z$  429.336, 505.315, 395.653, 441.299, 501.284, 443.314, 427.319, 429.336, 399.420, 517.351, 413.274, 471.875, and 503.254 were in agreement with the molecular formulas  $C_{28}H_{44}O_3$ ,  $C_{29}H_{46}O_7$ ,  $C_{28}H_{42}O$ ,  $C_{28}H_{40}O_4$ ,  $C_{29}H_{42}O_7$ ,  $C_{28}H_{42}O_4$ ,  $C_{28}H_{42}O_3$ ,  $C_{28}H_{44}O_3$ ,  $C_{27}H_{42}O_2$ ,  $C_{31}H_{48}O_6$ ,  $C_{30}H_{48}O_4$ , and  $C_{31}H_{50}O_5$ . They were dereplicated as erectasteroid H (5), pregn-20-ene-3,19-diol, (3 $\beta$ ,5 $\alpha$ ) form, 3-*O*-(3-*O*-acetyl- $\alpha$ -L-fucopyranoside) (6), ergosta-1,4,24(28)-trien-3-one (7), chabrolosteroid H (8), isogosterone B (9), chabrolosteroid G (11), chabrolosteroid E (14), chabrolosteroid C (15), cholest-1-ene-3,22-dione (16), nanjiol B (21), nephalsterol C (25), and nebrosteroid B (26), respectively.

Diterpenes with expected chemical formulas of  $C_{20}H_{28}O_2$  and mass ions of  $m/z$  221.376, 439.283, 271.346, 427.284, and 379.896 were dereplicated as nephthenol (1), chabrolbenzoquinone B (4), cembrene A (10), chabrolohydroxybenzoquinone F (13), and pacificin G (17), respectively.

Moreover, further fatty acid, providing the detected mass ions of  $m/z$  281.75449, 355.320, 311.054, 281.245, and 365.905, corresponding to the chemical formulas  $C_{18}H_{34}O_2$ ,  $C_{22}H_{44}O_3$ ,  $C_{20}H_{40}O_2$ ,  $C_{18}H_{32}O_2$ , and  $C_{24}H_{46}O_2$ , respectively, components were dereplicated as oleic acid (18), 2-hydroxydocosanoic acid (19), arachidic acid (20), linoleic acid (23), and nervonic acid (24), respectively.

The observed mass ions of  $m/z$  249.149 and 237.542 and the chemical formulas  $C_{15}H_{20}O_3$  and  $C_{15}H_{24}O_2$  evidenced the presence of the sesquiterpenes armatin F (3) and orientalol C (22), which have been identified earlier in *Nephthea* sp. [26].

A deprotonated molecule  $[M-H]^-$ , with an expected chemical formula of  $C_{36}H_{73}NO_4$  and a mass ion of  $m/z$  582.763, was identified as the ceramide nephtixamide B (27), while keto-chabrolic acid (2), which can be classified as a terpenoid-related carboxylic acid, appeared as a protonated molecule  $[M+H]^+$  with a mass ion of  $m/z$  293.227 and with a chemical formula of  $C_{18}H_{28}O_3$ . Also, the protonated molecule  $[M+H]^+$  bis(2-ethylhexyl)phthalate (12), with the chemical formula  $C_{24}H_{38}O_4$ , was detected with a mass ion of  $m/z$  392.539.

### Isolation of the Major Metabolites

Compound 12 was isolated and was identified as bis(2-ethylhexyl)phthalate (DEHP) with ESI-MS as well as  $^1H$  and  $^{13}C$  NMR analysis data [27]. The ESI-MS data presented a molecular ion peak at  $m/z$  391.42 and a base peak at 148.84 (calc. for  $C_{24}H_{38}O_4$ , 267.0657). Figure S2 shows the  $^1H$  and  $^{13}C$  NMR spectral data, which agree with findings of Elhagali et al., 2019 [28].

Figures S3 and S4 show the ESI-MS spectra of compounds 18 and 20, which were recognized as oleic acid and arachidic acid, respectively, by comparing the base peak with published data [29,30].

Based on characteristic signals in the  $^1H$  and  $^{13}C$  NMR spectra data and using comparison with the published data, compound 24 was identified as nervonic acid [31,32]. These data are displayed in Figure S5. This study is the first report on the isolation of these four compounds from the genus *Nephthea*.

### 2.3. Wound Healing Activity

The diabetic diagnostic was confirmed when the glucose level exceeded 300 mg/dL. During the experiments, the glucose level was monitored daily. The insulin was injected only when the level exceeded 500 mg/dL, in order to protect the rats against weakness and sudden death.

The current findings indicate that in all experimental groups, wound closure rates increased in a time-dependent manner. The wound closure percentages were about 18 to 20% in each group on day 3 after injury, with no discernible distinctions between the groups, with the lowest being in the untreated group and the highest in the treated ones. However, the wound closure in the SCN-LPN2-ISG-treated group reached 50% on day 6 after treatment, which was significantly higher than the corresponding untreated group; see Table 2 and Figures 7 and 8.



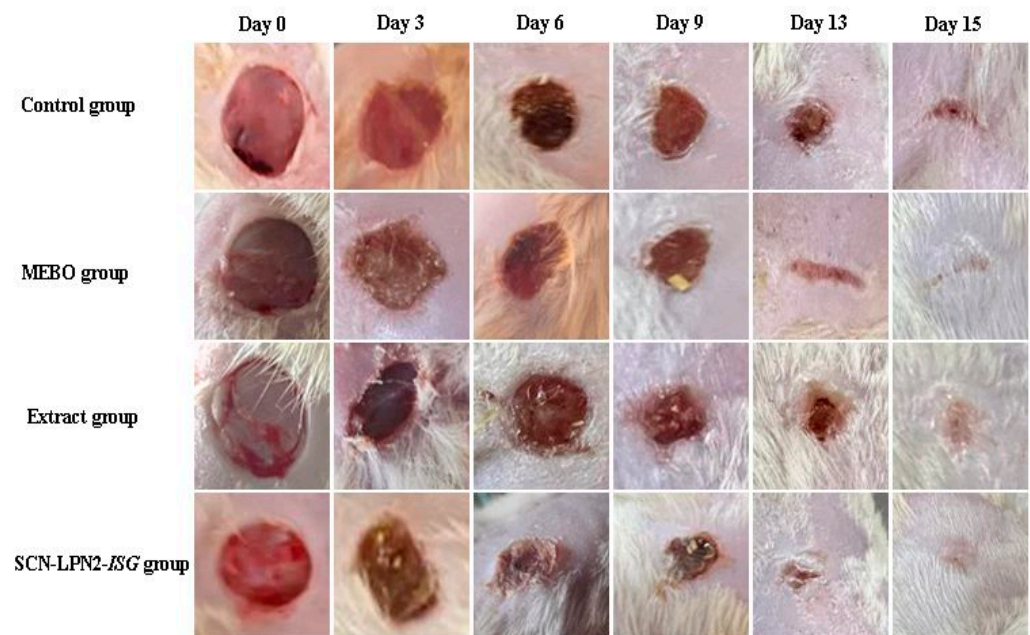
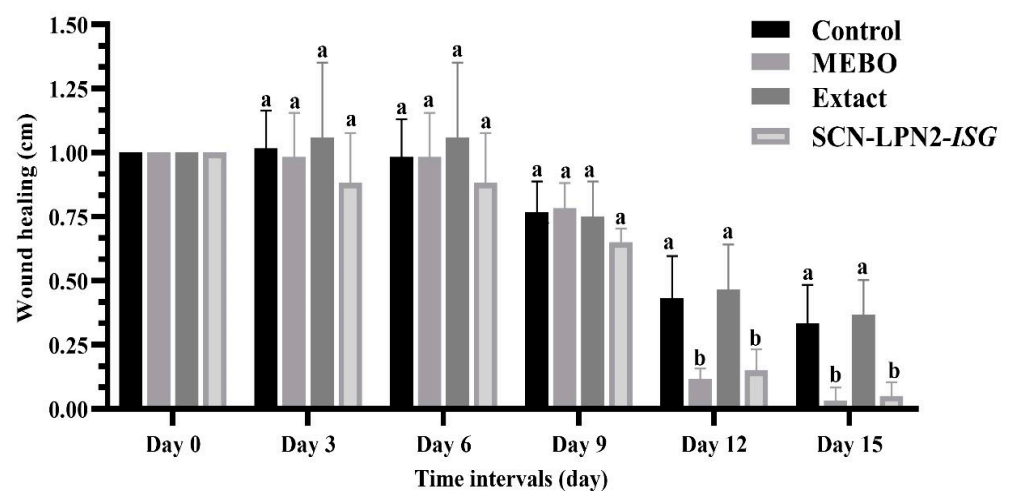
**Table 1.** Tentatively identified secondary metabolites identified in *Nephthea* sp. extract (using UPLC–Q/TOF–MS).

No.	Identified Metabolites	Molecular Formula	Rt. (min)	Ionization Mode	<i>m/z</i>	Molecular Weight	$\Delta$ Mass (ppm)	Chemical Class	References
1	Nephtenol	C <sub>15</sub> H <sub>26</sub> O	5.56	Negative	221.376520	222.198365	−2.3185972	Cembrane diterpene	[33]
2	Ketochabrolic acid	C <sub>18</sub> H <sub>28</sub> O <sub>3</sub>	5.75	Positive	293.227486	292.203803	−1.9893311	Terpenoid-related carboxylic acids	[34]
3	Armatin F	C <sub>15</sub> H <sub>20</sub> O <sub>3</sub>	6.48	Positive	249.149275	248.141930	2.7641515	Sesquiterpene	[26]
4	Chabrolobenzoquinone B	C <sub>28</sub> H <sub>38</sub> O <sub>4</sub>	7.79	Positive	439.283800	438.276500	−1.1620504	Diterpene	[34]
5	Erectasteroid H	C <sub>28</sub> H <sub>44</sub> O <sub>3</sub>	8.31	Positive	429.336642	428.328765	−0.6532361	Steroid	[26]
6	Pregn-20-ene-3,19-diol; (3 $\beta$ ,5 $\alpha$ )-form, 3-O-(3-O-acetyl- $\alpha$ - L-fucopyranoside)	C <sub>29</sub> H <sub>46</sub> O <sub>7</sub>	9.11	Negative	505.315812	506.323088	−2.5011635	Steroid	[14]
7	Ergosta-1,4,24(28)-trien-3-one	C <sub>28</sub> H <sub>42</sub> O	9.26	Positive	395.653219	394.323565	−1.9664193	Steroid	[35]
8	Chabrolosteroid H	C <sub>28</sub> H <sub>40</sub> O <sub>4</sub>	9.43	Positive	441.299122	440.291794	−1.9664193	Steroid	[34], [36]
9	Isogosterone B	C <sub>29</sub> H <sub>42</sub> O <sub>7</sub>	9.87	Negative	501.284708	502.291984	−2.1308277		
10	Cembrene A	C <sub>20</sub> H <sub>32</sub>	10.35	Negative	271.346700	272.250976	−2.8617931	Cembrane diterpene	[37]
11	Chabrolosteroid G	C <sub>28</sub> H <sub>42</sub> O <sub>4</sub>	10.41	Positive	443.314955	442.307657	−1.4758935	Steroid	[34]
12	Bis(2-ethylhexyl)phthalate *	C <sub>24</sub> H <sub>38</sub> O <sub>4</sub>	10.74	Positive	391.539732	390.426789	−2.9895325	Phthalates	[27]
13	Chabrolohydroxybenzoquinone F	C <sub>27</sub> H <sub>40</sub> O <sub>4</sub>	11.45	Negative	427.284428	428.291704	−2.2307176	Diterpene	[34]
14	Chabrolosteroid E	C <sub>28</sub> H <sub>42</sub> O <sub>3</sub>	11.56	Positive	427.319666	426.312288	−2.5948047	Steroid	[34]
15	Chabrolosteroid C	C <sub>28</sub> H <sub>44</sub> O <sub>3</sub>	12.04	Positive	429.336311	428.329034	−0.0238134		
16	Cholest-1-ene-3,22-dione	C <sub>27</sub> H <sub>42</sub> O <sub>2</sub>	12.35	Positive	399.420384	398.318485	0.4476480	Steroid	[14]
17	Pacificin G	C <sub>22</sub> H <sub>36</sub> O <sub>5</sub>	12.65	Negative	379.896542	380.256275	−1.3900752	Diterpene	[26]
18	Oleic acid *	C <sub>18</sub> H <sub>34</sub> O <sub>2</sub>	12.95	Negative	281.754231	282.586432	−2.0964387	Fatty acid	[15]
19	2-Hydroxydocosanoic acid	C <sub>22</sub> H <sub>44</sub> O <sub>3</sub>	13.26	Negative	355.320800	356.328077	−2.7163095	Fatty acid	[38]
20	Arachidic acid *	C <sub>20</sub> H <sub>40</sub> O <sub>2</sub>	13.58	Negative	311.054217	312.502653	−1.9700365	Fatty acid	[15]
21	Nanjiol B	C <sub>31</sub> H <sub>48</sub> O <sub>6</sub>	13.42	Positive	517.351338	516.343721	−2.6503592	Steroid	[26]
22	Orientalol C	C <sub>15</sub> H <sub>24</sub> O <sub>2</sub>	14.43	Positive	237.542987	236.177638	−2.5296721	Sesquiterpene	[39]
23	Linoleic acid	C <sub>18</sub> H <sub>32</sub> O <sub>2</sub>	14.86	Positive	281.245678	280.240232	1.5898976	Fatty acid	[15]
24	Nervonic acid *	C <sub>24</sub> H <sub>46</sub> O <sub>2</sub>	14.32	Negative	365.905392	366.219853	−2.9065342	Fatty acid	[15]
25	Nephalsteroid C	C <sub>30</sub> H <sub>48</sub> O <sub>4</sub>	15.39	Negative	471.875324	472.355263	−2.9850569	Steroid	[40]
26	Nebrosteroid B	C <sub>31</sub> H <sub>50</sub> O <sub>5</sub>	15.53	Positive	503.254835	502.365825	−0.2345662	Steroid	[14]
27	Nephtixamide B	C <sub>36</sub> H <sub>73</sub> NO <sub>4</sub>	16.46	Negative	582.763198	583.553959	−1.9956883	Ceramide	[18]

\* Compounds isolated in this study.

**Table 2.** Wound healing (%) in the experimental wounds at different time intervals.

Experimental Group Wounds	Wound Healing (%)				
	Day 3	Day 6	Day 9	Day 12	Day 15
Control (untreated)	−1.666	1.666	13.333	56.666	66.666
MEBO-treated group	1.666	1.666	21.666	88	98
Extract-treated group	−5.833	−5.833	25	48	60
SCN-LPN2-ISG group	11.666	11.666	35	75	90

**Figure 7.** Wound healing potential of SCN-LPN2-ISG (*in situ* gel loaded with nanoparticles) compared to the *Nephthea* sp. extract, MEBO, and untreated group in excisional wounds on days 0, 3, 6, 9, 12, and 15 post wounding.**Figure 8.** Area of wound (cm) in different treated groups, SCN-LPN2-ISG (*in situ* gel loaded with nanoparticles) compared to the *Nephthea* sp. extract, MEBO, and untreated group in excisional wounds on days 0, 3, 6, 9, 12, and 15 post wounding. Data are represented as the mean  $\pm$  SD ( $n = 6$ ). The different letters represent statistically significant differences ( $p < 0.01$ ) between treatment and control.

Additionally, the SCN-LPN2-ISG-treated group also showed high wound closure percentages compared to those of the *Nephthea* sp. extract and MEBO-treated group. The centripetal flow of the edges of a full-thickness wound to aid in wound tissue closure is referred to as wound closure. Figure 8 discloses the percentage of wound healing of the SCN-LPN2-ISG-treated group (80%) was significantly greater than that of the untreated group (50%) on the 13th day after injury. On day 15, the wounds in the treated groups were perfectly cured and the wound closure was 95% in the skin of rats that were treated with SCN-LPN2-ISG and 90% in the MEBO-treated group.

### 2.3.1. Histopathological Examination of Skin Tissue

The control healthy group (non-wounded) had no histopathological alteration and a normal histological structure of the epidermis with the underlying dermis with hair follicles and sebaceous glands followed by musculature and subcutaneous tissue (Figure 9A). On the other hand, Figure 9C shows the MEBO-treated group with a few underlying inflammatory cells' infiltration and granulation tissue formation as well as a loss of the hair follicle, and inflammatory cell infiltration was detected in subcutaneous tissue (Figure 9C). A mild focal acanthosis was detected in the epidermis of the SCN-LPN2-ISG group, while the underlying dermis showed formation of granulated tissue and a loss of hair follicles and sebaceous glands in association with a few infiltrations of inflammatory cells into the subcutaneous tissue (Figure 9E).

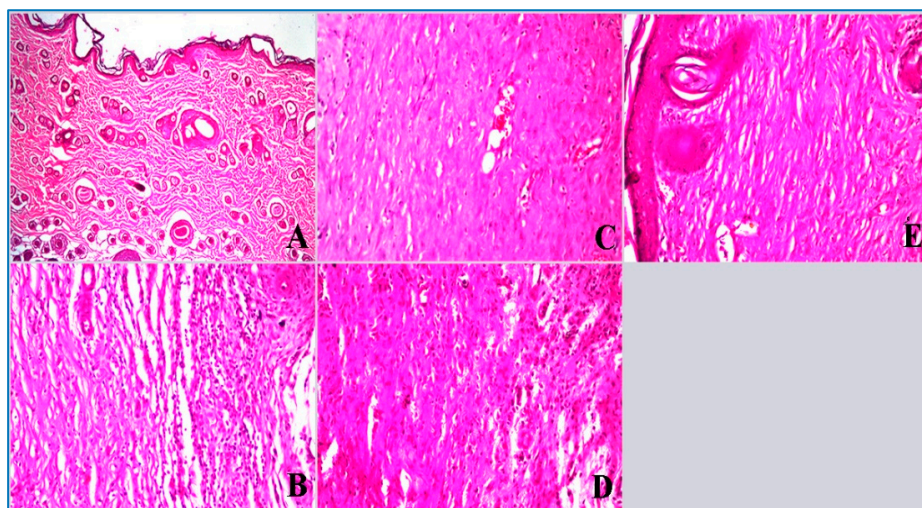


**Figure 9.** A representative photomicrograph of a section of the skin tissues stained with hematoxylin and eosin (H&E;  $\times 400$ ). Treated groups in comparison with the unwounded group (A), (B) untreated wounded group, (C) MEBO-treated group, (D) extract-treated group, (E) SCN-LPN2-ISG-treated group.

Moreover, the *Nephthea* sp. extract exposed a slight infiltration of inflammatory cells in the subcutaneous tissue and the deep dermis had granulation tissue formation with a loss of hair follicles (Figure 9D), compared with the untreated group, which showed focal necrosis in the epidermal and dermal layers with massive inflammatory cell infiltration (Figure 9B). According to these histological studies, SCN-LPN2-ISG and MEBO have a potent chronic wound healing effect.

### 2.3.2. Inflammation Markers

Inflammation is an evolutionarily settled process that allows for the defense of an organism against damage to its tissues and organs. The progression of wound inflammation is crucial for the optimal completion of hemostasis, as well as the detection and elimination of pathogenic microorganisms, the removal of damaged tissues, and wound cleaning [41]. These steps progress via the participation of leukocytes, which migrate from

the bloodstream to the site of injury. The migration is followed by the formation and release of pro-inflammatory cytokines and phagocytosis [42].

The current findings, as illustrated in Figure 10, show the inflammation response during the wound healing process under different treatments on days 7 and 15. The level of NF- $\kappa$ B was significantly decreased in groups designedly under treatment with the MEBO, extract, or SCN-LPN2-ISG compared to the untreated wounded group. Moreover, the TNF- $\alpha$  in the MEBO-treated group showed a non-significant difference compared with untreated wounded animals, while treatment with the extract and SCN-LPN2-ISG led to a significant decrease compared with untreated wounded animals on day 7; the same trend was found on day 15, with a noteworthy decrease when compared.

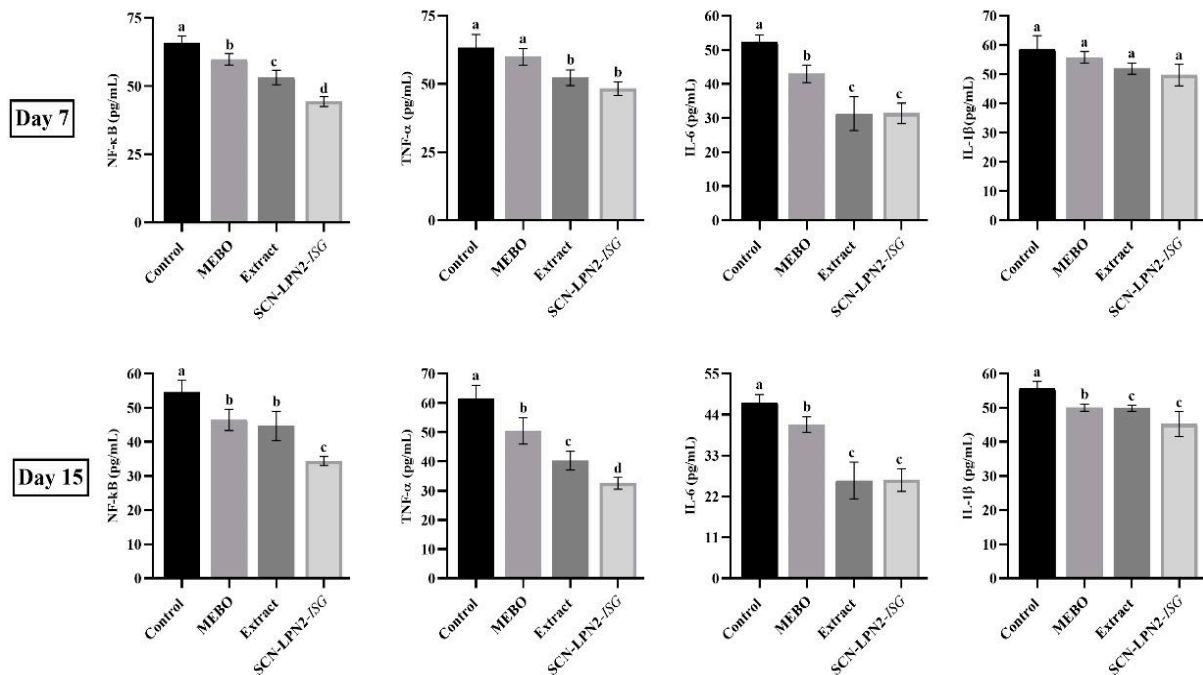


**Figure 10.** Protein levels of NF- $\kappa$ B, TNF- $\alpha$ , IL-6, and IL-1 $\beta$  in different experimental groups. Data represented as the mean  $\pm$  SD ( $n = 6$ ). SCN-LPN2-ISG = *in situ* gel loaded with nanoparticles; NF- $\kappa$ B = NF-kappa B; TNF $\alpha$  = tumor necrosis factor alpha; IL6 = interleukin 6; IL-1 $\beta$  = interleukin-1 beta; the different letters represent statistically significant differences ( $p < 0.05$ ) between treatment and control.

In the same trend, the treatment with the SCN-LPN2-ISG and extract caused a significant decrease in the IL-6 level when compared with MEBO-treated and untreated-wound groups; the same trend was noted on day 14. Furthermore, the different treatments did not cause any substantial different effects on the serum level of IL-1 $\beta$  on day 7, and the same trend was recorded on day 15, with a significant decrease ( $p < 0.05$ ).

Proinflammatory cytokines are among the first factors to be produced in response to skin wounds. They regulate the functions of immune cells in epithelialization. Proinflammatory cytokines, including TNF- $\alpha$ , are a central factor in the macrophage-promoted hair follicle telogen–anagen transition, and contribute to hair follicle neogenesis in skin wound healing [43]. Proinflammatory cytokines (TNF- $\alpha$ , IL-6, and IL-1 $\beta$ ) primarily play a pivotal role in acute wound healing by promoting the proliferation and antimicrobial peptide production of keratinocytes. An overproduction of proinflammatory cytokines, however, may lead to prolonged inflammation and wound healing. Therefore, blocking excessive proinflammatory cytokines exerts a therapeutic effect in chronic wound healing, which was observed to occur in the extract- and SCN-LPN2-ISG-treated groups; the effects may be attributed to anti-inflammatory active components that were found in the extract of the soft coral *Nephthea* sp. [44]. Inflammation is a vital action occurring during wound healing, and



it is necessary to remove the apoptotic cells from the damaged area [45]. According to the observation in Figures 7 and 10, the relation between the wound statuses was parallel with the level of inflammation markers. All tested inflammation protein was decreased at day 15 compared to them on day 7. The decrease in the inflammation markers was in parallel with the degree of the healing of wounds at the 15th day compared to them at the 7th day.

#### 2.4. In Vitro Inhibition Assay of GSK-3 and MMP-1 Enzymes

Rapid hemostasis, appropriate inflammation, mesenchymal cell differentiation, proliferation and migration to the wound site, suitable angiogenesis, prompt re-epithelialization, and proper collagen synthesis, cross-linking, and alignment are all pivotal requirements for optimal wound healing in healthy persons [3]. The strength of the rebuilding tissue is also the inhibition of glycogen synthase kinase 3 (GSK-3), a protein involved in energy metabolism, cell growth, and body pattern formation, which enhances wound healing via the  $\beta$ -catenin-dependent Wnt signaling pathway [46]. Both acute and chronic wounds include MMPs, which are categorized into eight families. They are essential for managing extracellular matrix deposition and breakdown, which is necessary for wound re-epithelialization.

The *Nephthea* sp. extract showed inhibitory activity towards GSK-3 compared with CHIR-99021 as a reference inhibitor, with  $IC_{50}$  values of  $0.178 \pm 0.009 \mu\text{g/mL}$  and  $0.065 \pm 0.003 \mu\text{g/mL}$ , respectively. Moreover, the enzymatic inhibition activity of the *Nephthea* sp. extract against MMP-1 opposing NNGH, with  $IC_{50}$  values of  $0.258 \pm 0.011 \mu\text{g/mL}$  and  $0.055 \pm 0.002 \mu\text{g/mL}$ , is illustrated in Figure 11.

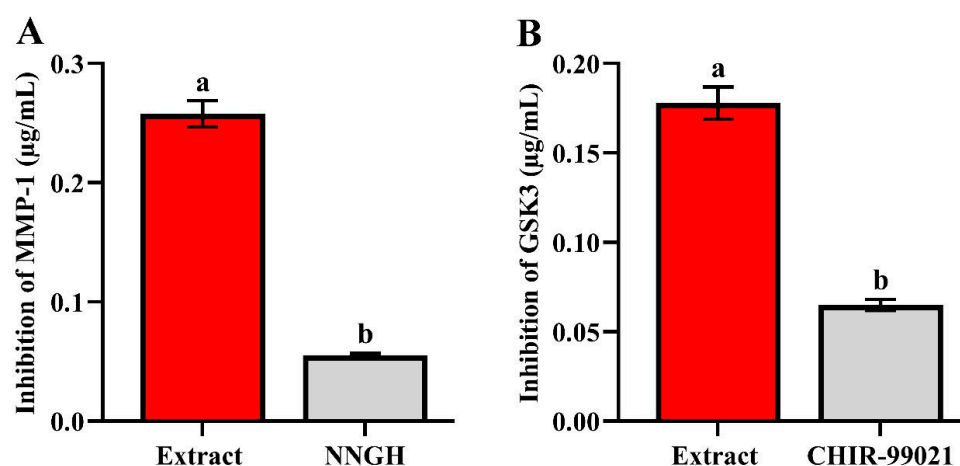


**Figure 11.** Inhibition activity ( $IC_{50}$ ) of the *Nephthea* sp. extract against (A) MMP-1 and (B) GSK-3 enzymes. Values are expressed as the mean  $\pm$  SD ( $n = 3$ ). Different letters (a and b) represent statistically significant differences ( $p < 0.05$ ) between extract and control.

#### 2.5. Molecular Docking

As a first step to further determine the mode of action of the identified compounds as potential wound healing agents, a molecular-docking study was performed to determine the binding modes against glycogen synthase kinase and matrix metalloproteinase-1. The co-crystallized ligands *N*-(4-methoxybenzyl)-*N'*-(5-nitro-1,3-thiazol-2-yl) urea (TMU) for GSK-3 and methylamino-phenylalanyl-leucyl-hydroxamic acid (PLH) for MMP-1 proteins were reduced to ensure the validity of the docking parameters and methods to represent the position and orientation of the ligand detected in the crystal structure. The difference in the RMSD value between co-crystal ligands and the original co-crystal ligands was  $<2 \text{ \AA}$ , which approved the accuracy of the docking protocols and parameters, as illustrated in Table 3 and Figures 12–15. All docking procedures and scoring were recorded according to our previous publications [47–49].

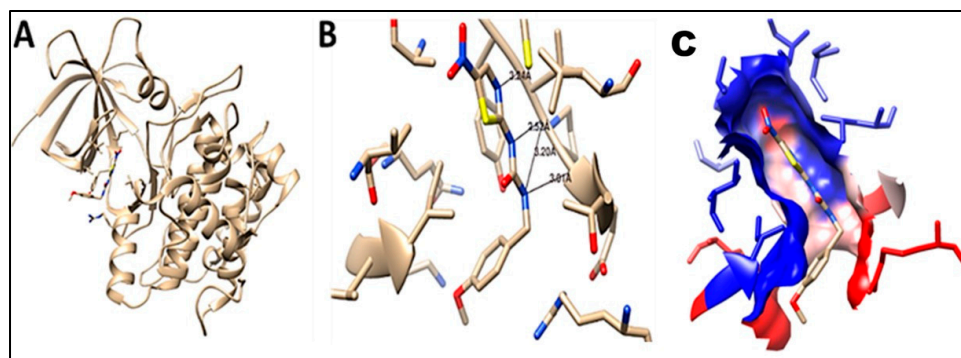


**Table 3.** Docking free binding energy score (kcal/mol) results of the detected compounds with UPLC–Q/TOF–MS of *Nephthea* sp. extract on the binding sites of GSK-3 and MMP-1, and corresponding co-crystallized ligands.

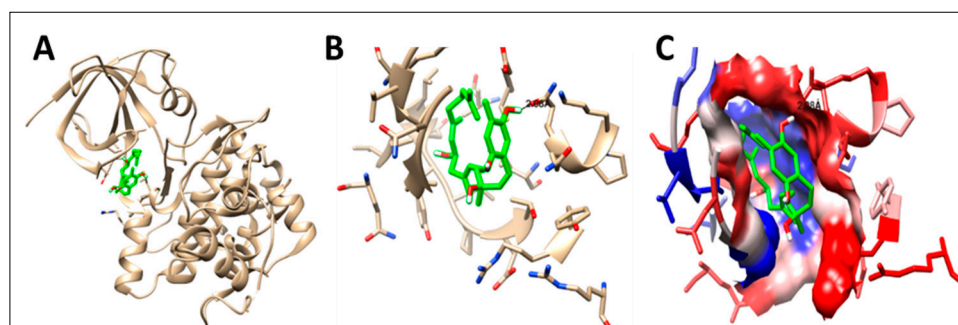
Compound		GSK-3 Protein (PDB: 1Q5K)			MMP-1 Protein (PDB: 1HFC)					
		Free Binding of Energy (Kcal/mol)	No. of H-Bonds	H-Bond Amino Acid Length Å	Free Binding of Energy (Kcal/mol)	No. of H-Bonds	H-Bond Amino Acid Length Å			
Co-crystallized ligand	<i>N</i> -(4-Methoxybenzyl)- <i>N'</i> -(5-nitro-1,3-thiazol-2-yl)urea (TMU)	−7.1	4	PRO136	3.01	−7.2	3	LEU181	3.17	
	VAL135			3.20	ASN180			3.14		
VAL135	2.52			TYR240	2.87					
VAL135	3.25			ASN180	2.94					
	Methylamino-phenylalanyl-leucyl-hydroxamic acid (PLH)		-----					TYR240	2.84	
	(1) 2-Hydroxydocosanoic acid	−5.5	–	–	–	−4.5	1	ASN180	2.94	
	(2) Armatin F	−6.9	1	GLN185	3.05	−6.0	1	SER172	2.97	
	(3) Chabrolobenzoquinone B	−7.6	2	ARG144	3.11	−6.4	3	TYR240	2.84	
				ARG144	3.17			LEU181	2.97	
	(4) Chabrolohydroxybenzoquinone F (13)	−8.2	1	ASN186	2.08	−7.4	3	LEU182	3.05	
				VAL135	3.37			GLY179	3.04	
				ARG144	3.15			GLY179	2.39	
	(5) Chabrolosteroid C	−6.9	2	ASN186	2.08	−7.1	3	LEU181	2.86	
				ARG144	3.15			GLY179	3.27	
	(6) Chabrolosteroid E	−9.6	1	GLN185	2.52	−5.7	2	LEU181	3.07	
				GLN185	2.52			LEU181	3.35	
<i>Nephthea</i> sp. identified metabolites	(7) Chabrolosteroid G	−7.5	1	CYS199	3.47	−7.1	5	GLY179	2.44	
								ELU181	3.07	
								LEU181	2.89	
								ALA182	2.81	
		(8) Chabrolosteroid H	−7.6	1	ILE62	2.00	−6.6	1	ALA182	2.03
		(9) Cholest-1-ene-3,22-dione	−7.0	-	-	-	−7.0	-	ASN180	2.88
		(10) Erectasteroid H	−7.2	1	ARG141	3.39	−6.8	-		
		(11) Ergosta-1,4,24(28)-trien-3-one	−7.2	1	TYR134	3.22	−7.1	1	SER172	2.95
		(12) Isogosterone B (9)	−6.0	1	ARG141	3.27	−7.8	2	ALA182	3.29
									LEU181	2.83
	(13) Ketoabrolic acid	−6.8	1	VAL135	3.09	−6.7	2	ALA187	2.32	
	(14) Linoleic acid	−5.6	1	CYS199	3.69	−5.8	1	TYR120	2.90	
	(15) Nanjiol B	−7.4	1	LYS183	3.19	−6.5	1	ARG214	3.07	
				VAL135	2.83			TYR240	3.19	
	(16) Nebrosteroid B	−8.0	3	GLN185	1.72	−5.7	2	ASN180	2.86	
				GLN185	2.69			ASN180	2.94	

Table 3. Cont.

Compound	GSK-3 Protein (PDB: 1Q5K)				MMP-1 Protein (PDB: 1HFC)			
	Free Binding of Energy (Kcal/mol)	No. of H-Bonds	H-Bond Amino Acid	Length Å	Free Binding of Energy (Kcal/mol)	No. of H-Bonds	H-Bond Amino Acid	Length Å
(17) Nephasterol C	−7.0	1	LYS85	2.86	−6.7	1	ALA184	2.40
(18) Nephthenol	−7.4	1	CYS199	3.68	−6.2	1	TYR240	3.21
(19) Nephtixamide B	−5.8	1	VAL135	3.16	−4.9	2	SER172	3.30
(20) Orientalol C	−7.3	-	-	-	−5.6	1	SER172	3.01
(21) Pacificin G	−7.9	3	VAL135	2.98	−6.1	3	TYR240	2.87
			GLN185	3.03			HIS183	3.04
			GLN185	2.91			LEU181	2.95
(21) Pacificin G	−7.9	3	VAL135	2.98	−6.1	3	ALA182	3.19
			GLN185	3.03			HIS183	3.04
			GLN185	2.91			LEU181	2.95
(22) Arachidic acid	−5.5	1	TYR134	3.02	−5.1	2	ALA182	3.19
			-	-			ARG214	3.11
			-	-			ARG214	3.00
(23) Nervonic A	−6.0	-	-	-	−5.4	2	ARG214	3.01
(24) Bis(2-ethylhexyl)phthalate	−6.4	1	CYS199	3.80	−5.9	1	ARG214	2.93
(25) Cembrene A	−9.4	-	-	-	−7.0	-	ASN180	2.91
(26) Oleic acid	−5.8	1	GLY68	2.12	−5.7	-	-	-
(27) Pregn-20-ene-3,19-diol; (3β,5α)-form; 3-O-(3-O-acetyl-α-L-fucopyranoside)			TYR134	2.99				
			ARG141	3.18				
			THR138	2.93				



**Figure 12.** Reference ligand (TMU) interaction with GSK-3 protein; (A) 3D interaction; (B) hydrogen bond formation; (C) hydrophobic interaction (in blue).



**Figure 13.** Chabrolohydroxybenzoquinone F (13) interaction with GSK-3 protein; (A) 3D interaction; (B) hydrogen bond formation; (C) hydrophobic interaction (in blue).

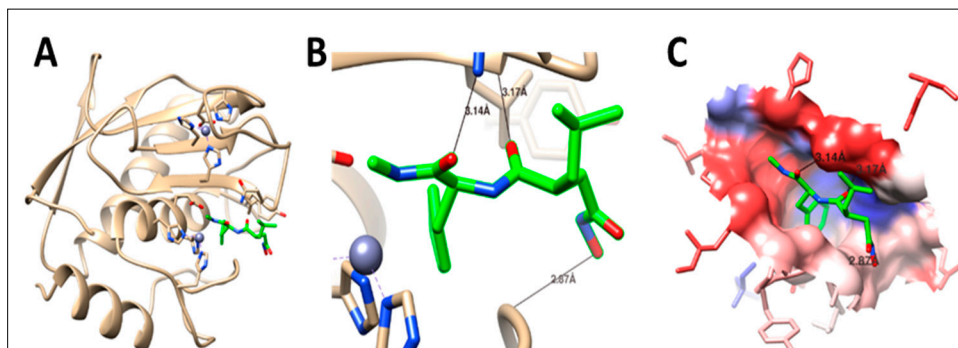


**Figure 14.** Reference ligand (PLH) interaction with MMP-1 protein; (A) 3D interaction; (B) hydrogen bond formation; (C) hydrophobic interaction (in blue).

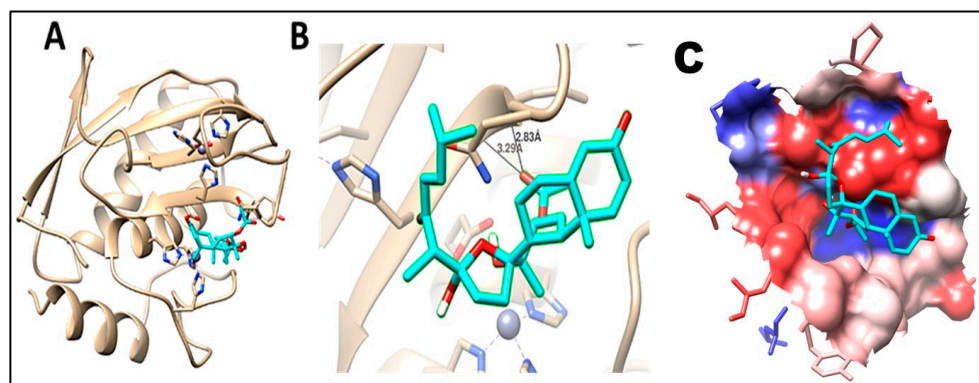


**Figure 15.** Isogosterone B (9) interaction with MMP-1 protein; (A) 3D interaction; (B) hydrogen bond formation; (C) hydrophobic interaction (in blue).

## 2.6. Physicochemical and ADME In Silico Study

Pharmacokinetic parameters should be incorporated with the significant filters, in order to further improve the chosen lead molecule transfer into drug candidates and permit lower failure rates in clinical trials because the majority of drug candidates fail during clinical development due to inadequate ADME features [17].

Based on docking results, the physicochemical properties and the drug likeness of the compounds chabrolohydroxybenzoquinone F (13) and isogosterone B (9) were studied. Moreover, ADME and toxicological studies were performed for these two promising compounds 9 and 13. The physicochemical properties of chabrolohydroxybenzoquinone F (13) and isogosterone B (9) were generated based on website data and are presented in a Bioavailability Radar Chart in Figure 16. The results depict that both compounds have excellent physicochemical properties and fulfil most of the criteria documented in Table 4. In addition, both compounds 9 and 13 showed acceptable medicinal–chemistry properties, drug likeness (fitting with the Lipinski and Pfizer rules), and ADME properties (see Supplementary Tables S2–S5).

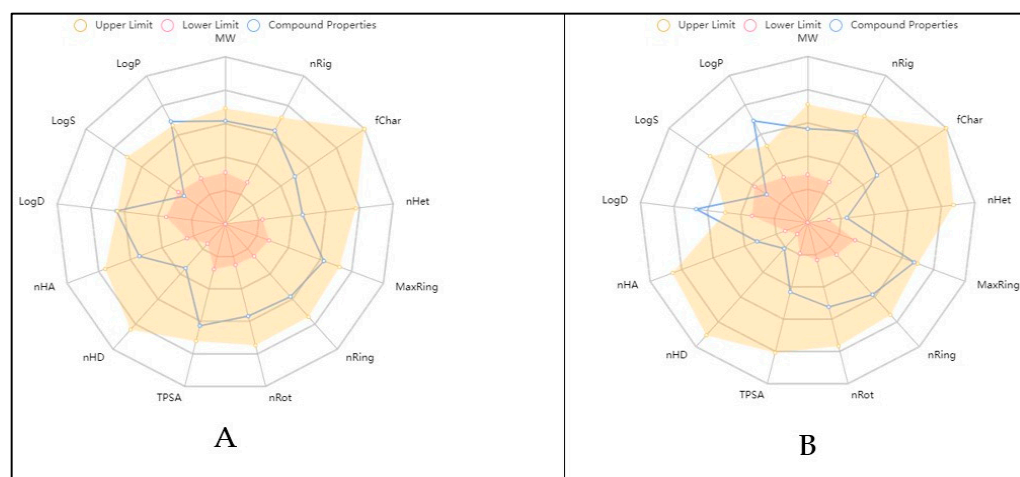


**Figure 16.** Bioavailability Radar, showing (A) chabrolohydroxybenzoquinone F (13) and (B) isogosterone B (9), represented by central blue lines fit in the pink area, which is the optimal range for each property.

**Table 4.** Physicochemical properties of the most potent compounds identified.

Parameter	Compounds		Comment
	Chabrolohydroxybenzoquinone F (13)	Isogosterone B (9)	
MW	428.290	502.290	No. of hydrogen atoms. Optimal: 100–600
nHA	4	7	No. of hydrogen bond acceptors. Optimal: 0–12
nHD	4	2	No. of hydrogen bond donors. Optimal: 0–7
TPSA	80.920	110.130	Topological polar surface area. Optimal: 0–140
nRot	11	7	No. of rotatable bonds. Optimal: 0–11
nRing	1	4	No. of rings. Optimal: 0–6
MaxRing	6	14	No. of atoms in the biggest ring. Optimal: 0–18
nHet	4	7	No. of heteroatoms. Optimal: 1–15
fChar	0	0	Formal charge. Optimal: –4
nRig	10	24	No. of rigid bonds. Optimal: 0–30
Flex	1.100	0.292	Flexibility = nRot/nRig
nStereo	2	8	No. of stereocenters. Optimal: ≤2
LogS	–3.650	–4.500	Log of aqueous solubility. Optimal: –4–0.5 log mol/L
LogD	4.452	3.036	Log of octanol/water partition coefficient. Optimal: 0–3
LogP	5.634	3.217	LogP at physiological pH 7.4. Optimal: 1–3

### 3. Materials and Methods

#### 3.1. Soft Coral Material and Chemicals

In January 2020, during snorkeling activity off the Red Sea coasts in Hurghada, Egypt, the soft coral *Nephthea* sp. was collected. Dr. El-Sayed Abed El-Aziz graciously provided an authentication for the specimen (Department of Invertebrates Lab., National Institute of Oceanography and Fisheries, Red Sea Branch, Hurghada, Egypt). The Pharmacognosy Department of the Faculty of Pharmacy at Deraya University created, maintained, and recorded the voucher specimen under the number NS-19-1-2020. Until examination, it was kept at  $-10\text{ }^{\circ}\text{C}$ . For marine extraction, analytical-grade solvents (methanol, methylene chloride) were used.

#### Extraction and Preparation

The frozen marine organism (500 g) was divided into smaller segments and was then repeatedly extracted using a methanol–methylene chloride (1:1) solution until it was completely exhausted. Finally, the solvent was evaporated using a rotary vacuum evaporator at a  $60\text{ }^{\circ}\text{C}$  water bath temperature, to yield 30 g of a concentrated extract.

#### 3.2. Metabolomic Profiling Study

Metabolomic fingerprinting was performed on the *Nephthea* sp. extract using an Acquity Ultra Performance Liquid Chromatography system coupled to a Synapt G2 HDMS quadrupole time-of-flight hybrid mass spectrometer (Waters, Milford, MA, USA), as discussed earlier (Hassan et al., 2022) [16].

Chromatographic separation was carried out on a BEH C18 column ( $2.1 \times 100\text{ mm}$ ,  $1.7\text{ }\mu\text{m}$  particle size; Waters, Milford, USA) with a guard column ( $2.1 \times 5\text{ mm}$ ,  $1.7\text{ }\mu\text{m}$  particle size) and a linear binary solvent gradient of 0–100% eluent B over 6 min at a flow rate of  $0.3\text{ mL min}^{-1}$ , using 0.1% formic acid in water (*v/v*) as solvent A and acetonitrile as solvent B. The injection volume was  $2\text{ }\mu\text{L}$  and the column temperature was  $40\text{ }^{\circ}\text{C}$ . To convert the raw data into separate positive and negative ionization files, MS Convert software was used. The files were then imported to the data mining software MZ mine 2.10 for peak picking, deconvolution, deisotoping, alignment, and formula prediction. The database used for compound identification was the Dictionary of Natural Products and Competitive Fragmentation Modeling for Metabolite Identification (CFM-ID) [18].

#### 3.3. Isolation of the Major Metabolites

Silica gel 60 (63–200 m, E. Merck, Sigma Aldrich, Germany) was used for column chromatography (CC), while silica gel GF254 for thin-layer chromatography (TLC) (El-Nasr Company for Pharmaceuticals and Chemicals, Cairo, Egypt) was employed for vacuum liquid chromatography (VLC). Pre-coated silica gel 60 GF<sub>254</sub> plates (E. Merck, Darmstadt, Germany;  $20 \times 20\text{ cm}$ , 0.25 mm in thickness) were used instead of thin-layer chromatography (TLC), which was driven out. Splashing with a *p*-anisaldehyde reagent (85:5:10:0.5, absolute ethanol: sulfuric acid: glacial acetic acid: *p*-anisaldehyde), followed by heating to  $110\text{ }^{\circ}\text{C}$ , was used to visualize spots [2]. For  $^1\text{H}$  and  $^{13}\text{C}$  NMR analyses, the following equipment was used: a Bruker AVIIIHD 400 FT-NMR spectrometer (400/3) from Japan. The measurements were made using  $\text{CDCl}_3$  as a deuterated solvent. The chemical shift values are represented in ppm (NMR Laboratory, Faculty of Pharmacy, Cairo University).

#### 3.4. Pharmaceutical Preparation

##### 3.4.1. Preparation and Characterization of Soft Coral *Nephthea* sp. Loaded with Pectin Nanoparticles (SCN-LPN)

Pectin from citrus or apple (galacturonic acid > 75%) was purchased from Fischer Scientific, USA. Calcium chloride ( $\text{CaCl}_2$ ), disodium hydrogen phosphate, potassium dihydrogen phosphate, potassium chloride, and sodium chloride were purchased from El-Nasr Chemical Company (Cairo, Egypt). A dialysis tubing cellulose membrane (12,000–14,000 molecular



weight cut-off) was purchased from Sigma Aldrich, Germany. Pluronic®F127 (PF127) and Pluronic®F68 (PF 68) were purchased from LOBA Chemie, India. Methanol absolute (99%) was purchased from the United Company for Chemical Medical Preparation (Cairo, Egypt).

#### Preparation of SCN-LPN

SCN-LPN was prepared with the ion-gelation technique with slight modification [20]. Briefly, 10 mL of a 0.5% *w/v* pectin solution was mixed with 3 mL of methanol (as the organic solvent), which contained 20 mg of the soft coral *Nephthea* sp. (SCN) extract. The above-described system was then treated drop-wise with an aqueous CaCl<sub>2</sub> solution (as a cross-linker) in different ratios, while being continuously stirred on a magnetic stirrer (Wisd WiseStir Lab, Instruments, UDA) for 30 min at 50 °C for 1000 rpm, until complete evaporation of the methanol, then filtrated through a filter membrane with a pore size of 0.45 µm. Table 5 lists the composition of various SCN-LPN formulations.

**Table 5.** Composition of various SCN-LPN formulations.

Formulation	Organic Phase		Aqueous Phases		Evaluation Parameters			
	SCN	Methanol	Pectin Concentration	Pectin: CaCl <sub>2</sub> Ratio	E.E. *	PS *	PDI *	ZP *
	(mg)	(mL)	(% <i>w/v</i> )		(%)	(nm)		(mV)
SCN-LPN1	20	3	0.5	1:1	92.84 ± 2.20	241.5 ± 17.5	0.290 ± 0.22	(−5.34) ± 1.20
SCN-LPN2	20	3	0.5	1:2	98.55 ± 2.20	288.2 ± 25.66	0.381 ± 0.12	(−16.6) ± 2.4
SCN-LPN3	20	3	0.5	1:3	97.55 ± 1.57	269.5 ± 34.7	0.523 ± 0.12	(−5.54) ± 1.5

N.B.: SCN: Soft coral *Nephthea* sp., E.E.: Entrapment efficiency, PS: Particle size, PDI: Polydispersity index, and ZP: Zeta potential. \* Data as mean values (n = 3) ± SD.

#### 3.4.2. Characterization of SCN-LPN

##### Determination of % SCN Entrapment Efficiency (% E.E.)

The % E.E. of SCN within the freshly prepared SCN-LPN was estimated indirectly by calculating the supernatant amount of SCN [25]. An aliquot of 1 mL of the freshly prepared SCN-LPN was centrifugated at 4 °C for 17,000 rpm for 30 min with cooling (PORISPIN 17R, Novapro Co. Ltd., Bucheon-si, Republic of Korea). The supernatant was separated and filtrated through a filter membrane (0.45 µm). The SCN was measured with a UV-visible spectrophotometer (JASCO, V-730, Japan) against methanol as a blank at a maximum wavelength ( $\lambda_{max}$ ) of 415 nm. The % E.E. was calculated using the following equation:

$$\% \text{ E.E.} = \frac{\text{total amount} - \text{unentrapped amount}}{\text{total amount}} \times 100 \quad (1)$$

##### Determination of Particle Size (PS), Polydispersity Index (PDI), and Zeta Potential (ZP)

Prior to measuring the PS and PDI, the freshly prepared SCN-LPN formulations (1.0 mL) were appropriately diluted with deionized water and vortexed to have a suitable scattering intensity. The ZP of the prepared SCN-LPN formulations was determined by observing their electrophoretic mobility in an electrical field, using a Malvern Zetasizer Nano (Nano-ZS, Malvern Instruments Ltd., Malvern, UK) at an angle of 90° in a 10 mm diameter cell at 25 °C [22].

##### Transmission Electron Microscopy (TEM)

Transmission electron microscopy (TEM, JEOL, JEM-1011, and Tokyo, Japan) was used to evaluate the size and the distribution of the prepared samples.

##### Fourier Transform Infrared Spectroscopy (FTIR)

The chemical nature of the prepared samples was recorded for the SCN extract, pectin, CaCl<sub>2</sub>, and selected lyophilized SCN-LPN formulation and unloaded formulation using a Fourier transform infrared (FTIR) spectrometer (VERTEX 80v, Bruker, Billerica, MA, USA).

### 3.4.3. Preparation and Characterization of Soft Coral *Nephthea* sp. Loaded with Pectin Nanoparticles *In-Situ* Gel (SCN-LPN-ISG)

#### Preparation of SCN-LPN-ISG

The cold method was used to prepare SCN-LPN-ISG with certain modifications [50]. In brief, 25% *w/v* of thermosensitive gel composed of a mixture of Pluronic® F127 (PF127) and Pluronic® F68 (PF68) in a suitable ratio was sprinkled over the selected SCN-LPN formulation, surrounded by an iced beaker at 4 °C and stirred at 400 rpm on a magnetic stirrer until a homogeneous system without lumps was obtained. The SCN-LPN-ISG thus obtained was stored overnight in a refrigerator for further studies.

### 3.4.4. Characterization of SCN-LPN-ISG

#### Visual Characterization, pH, and Drug Content (%) Analysis

The prepared SCN-LPN-ISG was visually checked for clarity, homogeneity, and color against a black and white background [51]. For pH measurement, a pH meter (Schott CG 840, Mainz, Germany) was used by dipping an electrode inside the prepared SCN-LPN-ISG. For the drug content analysis, 1 g from freshly prepared SCN-LPN-ISG was taken and suspended in 30 mL of PBS (pH = 7.4) with vigorous shaking for 12 h. The amount of SCN was measured spectrophotometrically against PBS (pH = 7.4) as a blank at  $\lambda_{\max} = 415$  nm, using a UV-Vis spectrophotometer. The drug content (%) was calculated using the following equation:

$$\text{Drug content (\%)} = \frac{\text{actual amount of SCN}}{\text{theoretical amount of SCN}} \times 100 \quad (2)$$

#### *Sol–Gel* Transformation Temperature

The inversion technique was used to detect the *sol–gel* transformation temperature [52]. The freshly prepared SCN-LPN-ISG (1.0 mL) was put into a sealed test tube. It was immersed in thermostatic water, while gradually raising the temperature from 25 °C to 37 °C, the temperature at which there was no movement of the liquid when the test tube was tilted up perpendicularly as recorded [53].

#### Rheology Properties

A cone and plate Brookfield viscometer (Model DV-III Rheometer, spindle CPE-40, Middleboro, MA, USA) with spindle (40) was used to estimate the viscosity of the freshly prepared SCN-LPN-ISG. It was measured at different temperatures (such as 25 °C and 37 °C), while varying the angular velocity between 1 rpm and 10 rpm. This was conducted to compare the viscosity before and after gelling formation [54].

### 3.5. *In Vitro* Release Studies

The percentage of the cumulatively released SCN amount during different time intervals from the prepared selected SCN-LPN and SCN-LPN-ISG formulations against SCN extract suspension was studied, using the dialysis tube technique. In brief, a specific amount from the prepared formulations was dispersed in 2 mL of PBS (pH = 7.4) and placed in a dialysis bag made of a cellophane membrane (12,000–14,000 molecular weight cut-off), which was blocked well at both ends. The dialysis bag was immersed in a beaker containing 500 mL of PBS (pH = 7.4), and stirred at a constant rate of 100 rpm on a magnetic stirrer at 37 °C for 8 h. An aliquot of the sample (3 mL) was withdrawn at specific time intervals (0.5, 1, 2, 3, 4, 5, 6, and 8 h) and replaced with fresh PBS (pH = 7.4). The amount of SCN released was measured spectrophotometrically against PBS (pH = 7.4) as a blank at  $\lambda_{\max} = 415$  nm, using a UV-visible spectrophotometer.

### 3.6. In Vivo Diabetic Wound Healing Study

#### 3.6.1. Experimental Animals and Ethical Statement

In this study, 24 male white Wistar rats weighing 100–120 g were utilized. They were purchased from the animal house of the Faculty of Science, Cairo University. The animals were housed separately, in steel mesh cages; kept under standard conditions—ventilation, temperature ( $25 \pm 2$  °C), humidity (60–70%), and light/dark conditions (12/12 h); and fed with a standard rat fresh diet along with clean drinking water. They were acclimatized for a period of 10 d before the beginning of this study. The rats were randomly divided into four groups (six rats each).

All surgical procedures and handling were approved by the research ethics committee of the Faculty of Pharmacy, Cairo University (Cairo, Egypt; under the number MP-3225) in compliance with the *Guide for the Care and Use of Laboratory Animals* published by the US National Institutes of Health, 8th edition (NIH Publication National Research, 2011). All efforts were made to minimize animal pain, discomfort, and suffering.

#### 3.6.2. Diabetic Model Induced

To induce type 2 diabetes in experimental rats, streptozotocin (STZ) was injected simultaneously with normal chow and a high-fat diet (60% calories as fat, 58Y1, Test Diet) for 2 weeks. A single intraperitoneal injection of 60 mg/kg STZ was given with a recovery high-fat diet during the experiment. The confirmation of the occurring type 2 diabetes in rats was ensured by measuring the blood glucose level with a glucometer (Accu-Chek Active, Berlin, Germany) 1 week after STZ injection [55].

#### 3.6.3. Circular Excision Wound Model

The back hair of all rats was shaved off. All rats were anesthetized with ether using inhalation before a full-thickness skin wound was made in the dorsum (in the subscapular area) using a 1 cm diameter punch. The dorsum position was selected to make the wound to ensure that they were inaccessible by the nails and the mouth, which prevented self-licking [56]. All rats were topically treated once daily day-after-day for 2 weeks.

1. **The first group** was considered as a control (untreated).
2. **In the second group**, the rats received a prepared extract of *Nephthea* sp. (applied as small pieces of sterile gauze macerated in 1.5 gm of the extract) and two pieces (30 mg) per wound dressing day-after-day for 15 d.
3. **The third group** received 1 cm from SCN-LPN-ISG (Conc.: 2 mg/mL), changed day-after-day for 15 d.
4. **The fourth group** served as a positive control, receiving MEBO ointment (as the market reference drug, 100 mg/wound, daily, Gulf Pharmaceutical Industries Company, Ras Al Khaimah, United Arab Emirates) day-after-day throughout the experiment period.

The blood samples were collected on days 7 and 15 and sera samples were isolated with centrifugation at 5000 rpm for 10 min and kept at 80 °C. The animals were euthanized, and skin tissues were taken at the end of the experiment.

#### 3.6.4. Wound Concentration Analysis

On days 0, 3, 6, 9, 12, and 15 of the experiment, each wound was photographed using a Sony DSC-WX70/P digital camera (Berlin, Germany) and a scale bar was used to measure the contraction of the injured area compared with the situation on day 0. By measuring the injured areas with specialized software for this morphometric study, the percentage of wound contraction for each rat was estimated using the formula below [57].

$$\text{Wound concentration (\%)} = \frac{[\text{initial wound area} - \text{analyzed area}]/\text{initial wound area}}{\times 100}$$

### 3.7. Histological and Histochemical Assessment Studies

Skin tissue samples (from wound sites) were taken from all rats in different groups and fixed in 10% formalin saline for 24 h. Washing was performed in tap water; then, they were subjected to dissimilarly serial dilutions of alcohol (methanol, ethanol, and absolute ethanol) that were used for dehydration. Specimens were cleared in xylene and embedded in paraffin at 56 °C in a hot-air oven for 24 h. Paraffin beeswax tissue blocks were prepared for sectioning at a 4–5 µm thickness with a rotary LEITZ microtome. The obtained tissue sections were collected on glass slides, deparaffinized, and stained with hematoxylin and eosin for examination through the light microscope [58].

### 3.8. Inflammatory Biomarker Assays

The levels of the nuclear factor kappa-light-chain-enhancer of activated B cells (NF-κB), interleukin 6 (IL-6), tumor necrosis factor-α (TNF-α), and interleukin-1β (IL-1β) in liver tissues were analyzed with ELISA kits obtained from Cusabio (Wuhan, China), as per the official manufacturer's method [59].

### 3.9. Inhibition Activity of *Nephthea* sp. Extract against GSK-3 and MMP-1 Enzymes (In Vitro)

To assess the inhibition activity of the *Nephthea* sp. extract against glycogen synthase kinase (GSK-3) and matrix metalloproteinase-1 (MMP-1) enzymes, CHIR-99021 and NNGH were used as positive reference inhibitors, respectively. The assay was carried out with kits of Kinase-Glo® (Promega Corporation, Madison, WI, USA) according to the procedure reported in the literature [60].

### 3.10. In Silico Studies

#### Molecular Docking and Pharmacokinetics, “ADME” Activity

The structures of all tested compounds were modeled using Chem Sketch software (<http://www.acdlabs.com/resources/freewar> (accessed on 19 January 2023)). The structures were optimized and energy minimized using VEGAZZ software [61]. The optimized compounds were used to perform molecular docking to elucidate the potential activity against glycogen synthase kinase (GSK-3) and matrix metalloproteinase-1 (MMP1), to analyze the proposed wound healing activity for the most promising compounds by targeting the enzyme. The three-dimensional structure of the molecular target was obtained from the Protein Data Bank (PDB) ([www.rcsb.org](http://www.rcsb.org) (accessed on 19 January 2023)): (PDB: 1Q5K, <https://www.rcsb.org/structure/1Q5K> (accessed on 19 January, 2023)), (PDB: <https://www.rcsb.org/structure/1HFC> (accessed on 19 January 2023)). The steps for receptor preparation included the removal of heteroatoms (water and ions), the addition of polar hydrogen, and the assignment of a charge. The active sites were defined using grid boxes of appropriate sizes around the bound co-crystal ligands. The docking study was performed using AutoDock Vina [62], and Chimera for visualization [63]. All docking procedures and scoring were recorded according to our previous publications [64].

To identify the biological targets for the most promising tested compounds, we employed searching in a database function integrated into Swiss Institute Bioinformatics tools [65]. Further, absorption, distribution, metabolism, and excretion “ADME” were hypothetically calculated [66].

### 3.11. Statistical Analysis

All experiments were conducted in triplicate, and the data are expressed as the mean ± SD. The one-way analysis of variance (ANOVA) was followed by the Duncan test to calculate statistical differences between the different treatments.  $p < 0.05$  means that there was a significant difference between the data. GraphPad Prism 8.0 (GraphPad Prism Software Inc., San Diego, CA, USA) was used to visualize the results. Statistical differences in the wound healing area at  $p < 0.01$  were observed between the treatment and control groups.

#### 4. Conclusions

Herein for the first time, the preparation and characterization of a polymeric (pectin) nanoparticle-loaded marine soft coral *Nephthea* sp. extract is reported. An *in situ* gel formula was formed to determine its potential stimulation activity toward diabetic wound healing. The UPLC-Q/TOF-MS fingerprint of the extract represents the secondary metabolite profile of the soft coral. This is the first documentation of the isolation of three fatty acids and one phthalate compound from *Nephthea* sp. *In silico* and ADME studies of the identified compounds evidenced their mechanism of action to be a wound healing enhancer. Our results indicate that *Nephthea* sp. is a rich source of effective metabolites, making it a promising candidate as a wound healing drug. We hope that this work will raise awareness of natural marine sources that can be used to speed up the healing of chronic diabetic wounds and encourage further clinical trials to evaluate the safety of *in situ* gel nanoparticles against synthetic medications to treat chronic wounds.

**Supplementary Materials:** The following supporting information can be downloaded at: <https://www.mdpi.com/article/10.3390/ph16070957/s1>, Figure S1. Total ion chromatogram of *Nephthea* sp. extract recorded in (A) positive ionization mode and (B) negative ionization mode. Figure S2. ESI-MS as well as <sup>1</sup>H NMR and <sup>13</sup>C NMR spectra of compound 12 (bis-(2-ethylhexyl)-phthalate) measured in CDCl<sub>3</sub>. Figure S3. ESI-MS spectra of compound 18 (oleic acid) measured in CDCl<sub>3</sub>. Figure S4. ESI-MS spectra of compound 20 (arachidic acid) measured in CDCl<sub>3</sub>. Figure S5. <sup>1</sup>H NMR and <sup>13</sup>C NMR spectra of compound 24 (nervonic acid) measured in CDCl<sub>3</sub>. Table S1. Medicinal–chemistry properties for the most active compounds. Table S2. Absorption profile for the most active compounds. Table S3. Distribution properties for the most active compounds. Table S4. Metabolism profile for the most active compounds. Table S5. Excretion for the most active compounds.

**Author Contributions:** Conceptualization, N.H.H., G.B., R.M.A.A.-E., M.A.R. and M.S.; methodology, M.E., M.A.R. and S.S.E.-H.; software, M.S., U.R.A. and M.A.T.; validation, U.R.A. and N.M.S.; writing—original draft preparation, N.H.H. and R.M.A.A.-E.; writing—review and editing, M.E., U.R.A. and G.B.; project administration, N.H.H.; funding acquisition, M.A.R. All authors have read and agreed to the published version of the manuscript.

**Funding:** Authors extend their appreciation to the Deanship of Scientific Research at King Khalid University. This research work was funded by the Small Group Research Project under the grant number RGP1/165/44.

**Institutional Review Board Statement:** All surgical procedures and handling were approved by the research ethics committee of the Faculty of Pharmacy, Cairo University (Cairo, Egypt; under the number MP-3225) in compliance with the Guide for the Care and Use of Laboratory Animals published by the US National Institutes of Health, 8th edition (NIH Publication National Research, 2011).

**Informed Consent Statement:** Not applicable.

**Data Availability Statement:** Data is contained within this article and Supplementary Material.

**Conflicts of Interest:** The authors declare no conflict of interest.

#### References

1. Bonilla-Escobar, F.J.; Gutiérrez, M.I. Injuries are not accidents: Towards a culture of prevention. *Colomb. Med.* **2014**, *45*, 132–135. [[CrossRef](#)]
2. Al-Warhi, T.; Zahran, E.M.; Selim, S.; Al-Sanea, M.M.; Ghoneim, M.M.; Maher, S.A.; Mostafa, Y.A.; Alsenani, F.; Elrehany, M.A.; Almuhayawi, M.S. Antioxidant and wound healing potential of vitis vinifera seeds supported by phytochemical characterization and docking studies. *Antioxidants* **2022**, *11*, 881. [[CrossRef](#)] [[PubMed](#)]
3. Guo, S.a.; DiPietro, L.A. Factors affecting wound healing. *J. Dent. Res.* **2010**, *89*, 219–229. [[CrossRef](#)] [[PubMed](#)]
4. Tenci, M.; Rossi, S.; Bonferoni, M.C.; Sandri, G.; Boselli, C.; Di Lorenzo, A.; Daglia, M.; Cornaglia, A.I.; Gioglio, L.; Perotti, C. Particulate systems based on pectin/chitosan association for the delivery of manuka honey components and platelet lysate in chronic skin ulcers. *Int. J. Pharm.* **2016**, *509*, 59–70. [[CrossRef](#)]
5. Soubhagya, A.; Moorthi, A.; Prabakaran, M. Preparation and characterization of chitosan/pectin/zno porous films for wound healing. *Int. J. Biol. Macromol.* **2020**, *157*, 135–145. [[CrossRef](#)] [[PubMed](#)]



6. Emam, M.; El Raey, M.A.; Eisa, W.H.; El-Haddad, A.E.; Osman, S.M.; El-Ansari, M.A.; Rabie, A.-G.M. Green synthesis of silver nanoparticles from caesalpinia gilliesii (hook) leaves: Antimicrobial activity and in vitro cytotoxic effect against bj-1 and mcf-7 cells. *J. Appl. Pharm. Sci.* **2017**, *7*, 226–233.
7. Marimuthu, S.; Rahuman, A.A.; Kirthi, A.V.; Santhoshkumar, T.; Jayaseelan, C.; Rajakumar, G. Eco-friendly microbial route to synthesize cobalt nanoparticles using bacillus thuringiensis against malaria and dengue vectors. *Parasitol. Res.* **2013**, *112*, 4105–4112. [[CrossRef](#)]
8. Saratale, R.G.; Karuppusamy, I.; Saratale, G.D.; Pugazhendhi, A.; Kumar, G.; Park, Y.; Ghodake, G.S.; Bharagava, R.N.; Banu, J.R.; Shin, H.S. A comprehensive review on green nanomaterials using biological systems: Recent perception and their future applications. *Colloids Surf. B Biointerfaces* **2018**, *170*, 20–35. [[CrossRef](#)]
9. Bera, S.; Mitra, R.; Singh, J. Recent advancement in protected delivery methods for carotenoid: A smart choice in modern nutraceutical formulation concept. *Biotechnol. Genet. Eng. Rev.* **2023**, 1–57. [[CrossRef](#)]
10. Liu, Y.; Weng, P.; Liu, Y.; Wu, Z.; Wang, L.; Liu, L. Citrus pectin research advances: Derived as a biomaterial in the construction and applications of micro/nano-delivery systems. *Food Hydrocoll.* **2022**, *133*, 107910. [[CrossRef](#)]
11. Ishihara, M.; Kishimoto, S.; Nakamura, S.; Sato, Y.; Hattori, H. Polyelectrolyte complexes of natural polymers and their biomedical applications. *Polymers* **2019**, *11*, 672. [[CrossRef](#)] [[PubMed](#)]
12. Kumar, P.; Kumar, V.; Kumar, R.; Pruncu, C.I. Fabrication and characterization of ceftizoxime-loaded pectin nanocarriers. *Nanomaterials* **2020**, *10*, 1452. [[CrossRef](#)] [[PubMed](#)]
13. Alexander, A.; Saraf, S.; Saraf, S. Understanding the role of poloxamer 407 based thermoreversible in situ gelling hydrogel for delivery of pegylated melphalan conjugate. *Curr. Drug Deliv.* **2016**, *13*, 621–630. [[CrossRef](#)] [[PubMed](#)]
14. Abdelhafez, O.H.; Fahim, J.R.; Desoukey, S.Y.; Kamel, M.S.; Abdelmohsen, U.R. Recent updates on corals from nephtheidae. *Chem. Biodivers.* **2019**, *16*, e1800692. [[CrossRef](#)]
15. Hassan, N.H.; El-Hawary, S.S.; Emam, M.; Rabeh, M.A.; Abdelmohsen, U.R.; Selim, N.M. Potential inhibitors of cyp51 enzyme in dermatophytes by red sea soft coral *Nephthea* sp.: In silico and molecular networking studies. *ACS Omega* **2022**, *7*, 13808–13817. [[CrossRef](#)]
16. Hassan, N.H.; Elhawary, S.; Emam, M.; Rabeh, M.A.; Muhsinah, A.B.; Asiri, Y.I.; Hamed, E.A.; Abdelmohsen, U.R.; Selim, N.M. Bioactive constituents of marine soft coral *Nephthea* sp. Against herpes simplex type i (hsv-1) and coxsackie b4 (coxb4) viruses; in-vitro and in silico studies. *Egypt. J. Chem.* **2022**. [[CrossRef](#)]
17. Hassan, N.H.; El-Hawary, S.S.; Emam, M.; Safwat, N.A.; Rabeh, M.A.; Abdelmohsen, U.R.; Selim, N.M. *Nephthea* sp. Inhibits biofilm, DNA gyrase, hsp90, and dhfr: In vitro, in silico, and pharmacokinetics studies. *Nat. Prod. Res.* **2022**, 1–6. [[CrossRef](#)]
18. Abdelhafez, O.H.; Fahim, J.R.; Mustafa, M.; AboulMagd, A.M.; Desoukey, S.Y.; Hayallah, A.M.; Kamel, M.S.; Abdelmohsen, U.R. Natural metabolites from the soft coral *Nephthea* sp. As potential SARS-COV-2 main protease inhibitors. *Nat. Prod. Res.* **2022**, *36*, 2893–2896. [[CrossRef](#)]
19. Hamed, A.; Abdel-Razek, A.S.; Araby, M.; Abu-Elghait, M.; El-Hosari, D.G.; Frese, M.; Soliman, H.S.; Stammeler, H.G.; Sewald, N.; Shaaban, M. Meleagrins from marine fungus *emerella dentata* nq45: Crystal structure and diverse biological activity studies. *Nat. Prod. Res.* **2021**, *35*, 3830–3838. [[CrossRef](#)]
20. Yener, S.; Akbulut, K.G.; Karakuş, R.; Erdoğan, D.; Acartürk, F. Development of melatonin loaded pectin nanoparticles for the treatment of inflammatory bowel disease: In vitro and in vivo studies. *J. Drug Deliv. Sci. Technol.* **2022**, *67*, 102861. [[CrossRef](#)]
21. Oveissi, F.; Tavakoli, N.; Minaiyan, M.; Mofid, M.R.; Taheri, A. Alginate hydrogel enriched with ambystoma mexicanum epidermal lipoxigenase-loaded pectin nanoparticles for enhanced wound healing. *J. Biomater. Appl.* **2020**, *34*, 1171–1187. [[CrossRef](#)]
22. Abd-Elal, R.M.; Shamma, R.N.; Rashed, H.M.; Bendas, E.R. Trans-nasal zolmitriptan novasomes: In-vitro preparation, optimization and in-vivo evaluation of brain targeting efficiency. *Drug Deliv.* **2016**, *23*, 3374–3386. [[CrossRef](#)] [[PubMed](#)]
23. Abd-Elal, R.M.; Elosaily, G.H.; Gad, S.; Khafagy, E.-S.; Mostafa, Y. Full factorial design, optimization, in vitro and ex vivo studies of ocular timolol-loaded microsponges. *J. Pharm. Innov.* **2020**, *15*, 651–663. [[CrossRef](#)]
24. Ghasemi, S.; Jafari, S.M.; Assadpour, E.; Khomeiri, M. Production of pectin-whey protein nano-complexes as carriers of orange peel oil. *Carbohydr. Polym.* **2017**, *177*, 369–377. [[CrossRef](#)] [[PubMed](#)]
25. Chinnaiyan, S.K.; Karthikeyan, D.; Gadela, V.R. Development and characterization of metformin loaded pectin nanoparticles for t2 diabetes mellitus. *Pharm. Nanotechnol.* **2018**, *6*, 253–263. [[CrossRef](#)] [[PubMed](#)]
26. Amir, F.; Koay, Y.C.; Yam, W.S. Chemical constituents and biological properties of the marine soft coral nephthea: A review (part 1). *Trop. J. Pharm. Res.* **2012**, *11*, 485–498.
27. Priya, A.M.; Jayachandran, S. Induction of apoptosis and cell cycle arrest by bis (2-ethylhexyl) phthalate produced by marine bacillus pumilus mb 40. *Chem.-Biol. Interact.* **2012**, *195*, 133–143. [[CrossRef](#)]
28. Elhagali, G.A.; Abozeed, A.E.; Youssif, Y.M. Investigation of bioactive constituents and biological activities of different fractions from herniaria hemistemon J. Gay. *Al-Azhar Bull. Sci.* **2019**, *30*, 67–80. [[CrossRef](#)]
29. Abbas, A.S.; Abbas, S.M. Kinetic study and simulation of oleic acid esterification in different type of reactors. *Iraqi J. Chem. Pet. Eng.* **2013**, *14*, 13–20.
30. Termsarasab, U.; Cho, H.-J.; Kim, D.H.; Chong, S.; Chung, S.-J.; Shim, C.-K.; Moon, H.T.; Kim, D.-D. Chitosan oligosaccharide-arachidic acid-based nanoparticles for anti-cancer drug delivery. *Int. J. Pharm.* **2013**, *441*, 373–380. [[CrossRef](#)]
31. Li, Q.; Chen, J.; Yu, X.; Gao, J.-M. A mini review of nervonic acid: Source, production, and biological functions. *Food Chem.* **2019**, *301*, 125286. [[CrossRef](#)] [[PubMed](#)]

32. Giwa, A.S.; Ali, N. Perspectives of nervonic acid production by *Yarrowia lipolytica*. *Biotechnol. Lett.* **2022**, *44*, 193–202. [[CrossRef](#)] [[PubMed](#)]
33. Ishii, T.; Kamada, T.; Vairappan, C.S. Three new cembranoids from the bornean soft coral *Nephthea* sp. *J. Asian Nat. Prod. Res.* **2016**, *18*, 415–422. [[CrossRef](#)]
34. Amir, F.; Koay, Y.C.; Yam, W.S. Chemical constituents and biological properties of the marine soft coral *Nephthea*: A review (part 2). *Trop. J. Pharm. Res.* **2012**, *11*, 499–517.
35. Yan, X.-H.; Liu, H.-L.; Huang, H.; Li, X.-B.; Guo, Y.-W. Steroids with aromatic a-rings from the hainan soft coral *Dendronephthya studeri* ridley. *J. Nat. Prod.* **2011**, *74*, 175–180. [[CrossRef](#)] [[PubMed](#)]
36. Sarma, N.S.; Krishna, M.S.; Pasha, S.G.; Rao, T.S.P.; Venkateswarlu, Y.; Parameswaran, P. Marine metabolites: The sterols of soft coral. *Chem. Rev.* **2009**, *109*, 2803–2828. [[CrossRef](#)]
37. Ishii, T.; Zhaoqi, Z.; Vairappan, C.S. A new cembrane diterpene from the bornean soft coral *Nephthea* sp. *Molecules* **2010**, *15*, 3857–3862. [[CrossRef](#)]
38. Farokhi, F.; Wielgosz-Collin, G.; Clement, M.; Kornprobst, J.-M.; Barnathan, G. Cytotoxicity on human cancer cells of ophidiacerebrosides isolated from the african starfish *Narcissia canariensis*. *Mar. Drugs* **2010**, *8*, 2988–2998. [[CrossRef](#)]
39. Fraga, B.M. Natural sesquiterpenoids. *Nat. Prod. Rep.* **2010**, *27*, 1681–1708. [[CrossRef](#)]
40. Hsiao, T.-H.; Cheng, C.-H.; Wu, T.-Y.; Lu, M.-C.; Chen, W.-F.; Wen, Z.-H.; Dai, C.-F.; Wu, Y.-C.; Sung, P.-J. New cembranoid diterpenes from the cultured octocoral *Nephthea columnaris*. *Molecules* **2015**, *20*, 13205–13215. [[CrossRef](#)]
41. Serra, M.B.; Barroso, W.A.; Silva, N.N.d.; Silva, S.d.N.; Borges, A.C.R.; Abreu, I.C.; Borges, M.O.d.R. From inflammation to current and alternative therapies involved in wound healing. *Int. J. Inflamm.* **2017**, *2017*, 3406215. [[CrossRef](#)]
42. Akita, S. Wound repair and regeneration: Mechanisms, signaling. *Int. J. Mol. Sci.* **2019**, *20*, 6328. [[CrossRef](#)]
43. Wang, X.; Chen, H.; Tian, R.; Zhang, Y.; Drutskaya, M.S.; Wang, C.; Ge, J.; Fan, Z.; Kong, D.; Wang, X. Macrophages induce akt/ $\beta$ -catenin-dependent Igr5+ stem cell activation and hair follicle regeneration through tnf. *Nat. Commun.* **2017**, *8*, 14091. [[CrossRef](#)]
44. Ashcroft, G.S.; Jeong, M.J.; Ashworth, J.J.; Hardman, M.; Jin, W.; Moutsopoulos, N.; Wild, T.; McCartney-Francis, N.; Sim, D.; McGrady, G. Tumor necrosis factor- $\alpha$  (tnf- $\alpha$ ) is a therapeutic target for impaired cutaneous wound healing. *Wound Repair Regen.* **2012**, *20*, 38–49. [[CrossRef](#)]
45. Rai, N.K.; Tripathi, K.; Sharma, D.; Shukla, V.K. Apoptosis: A basic physiologic process in wound healing. *Int. J. Low Extrem. Wounds* **2005**, *4*, 138–144. [[CrossRef](#)]
46. Ahamed, K.B.; Gowdru, H.B.; Rajashekarappa, S.; Malleshappa, K.S.H.; Krishna, V. Molecular docking of glycogen synthase kinase3- $\beta$  inhibitor oleanolic acid and its wound-healing activity in rats. *Med. Chem. Res.* **2013**, *22*, 156–164. [[CrossRef](#)]
47. Tantawy, M.A.; Shalby, A.B.; Barnawi, I.O.; Kattan, S.W.; Abd-Rabou, A.A.; Elmegeed, G.A. Anti-cancer activity, and molecular docking of novel hybrid heterocyclic steroids revealed promising anti-hepatocellular carcinoma agent: Implication of cyclin dependent kinase-2 pathway. *Steroids* **2023**, *193*, 109187. [[CrossRef](#)]
48. Qin, C.; Li, Y.; Zhang, Y.; Liu, L.; Wu, Z.; Weng, P. Insights into oat polyphenols constituent against advanced glycation end products mechanism by spectroscopy and molecular interaction. *Food Biosci.* **2021**, *43*, 101313. [[CrossRef](#)]
49. Abdelshaheed, M.M.; El Subbagh, H.I.; Tantawy, M.A.; Attia, R.T.; Youssef, K.M.; Fawzy, I.M. Discovery of new pyridine heterocyclic hybrids; design, synthesis, dynamic simulations, and in vitro and in vivo breast cancer biological assays. *RSC Adv.* **2023**, *13*, 15689–15703. [[CrossRef](#)]
50. Gupta, S.; Shende, P. L-proline adsorbed oxygen-loaded nanobubbles in-situ gel for wound healing. *Colloids Surf. A Physicochem. Eng. Asp.* **2022**, *647*, 129028. [[CrossRef](#)]
51. Kurniawansyah, I.S.; Rusdiana, T.; Sopyan, I.; Ramoko, H.; Wahab, H.A.; Subarnas, A. In situ ophthalmic gel forming systems of poloxamer 407 and hydroxypropyl methyl cellulose mixtures for sustained ocular delivery of chloramphenicol: Optimization study by factorial design. *Heliyon* **2020**, *6*, e05365. [[CrossRef](#)]
52. Lu, C.; Liu, M.; Fu, H.; Zhang, W.; Peng, G.; Zhang, Y.; Cao, H.; Luo, L. Novel thermosensitive in situ gel based on poloxamer for uterus delivery. *Eur. J. Pharm. Sci.* **2015**, *77*, 24–28. [[CrossRef](#)]
53. Rarokar, N.R.; Saoji, S.D.; Raut, N.A.; Taksande, J.B.; Khedekar, P.B.; Dave, V.S. Nanostructured cubosomes in a thermoresponsive depot system: An alternative approach for the controlled delivery of docetaxel. *AAPS PharmSciTech* **2016**, *17*, 436–445. [[CrossRef](#)] [[PubMed](#)]
54. Kesarla, R.; Tank, T.; Vora, P.A.; Shah, T.; Parmar, S.; Omri, A. Preparation and evaluation of nanoparticles loaded ophthalmic in situ gel. *Drug Deliv.* **2016**, *23*, 2363–2370. [[CrossRef](#)] [[PubMed](#)]
55. Mansor, L.S.; Gonzalez, E.R.; Cole, M.A.; Tyler, D.J.; Beeson, J.H.; Clarke, K.; Carr, C.A.; Heather, L.C. Cardiac metabolism in a new rat model of type 2 diabetes using high-fat diet with low dose streptozotocin. *Cardiovasc. Diabetol.* **2013**, *12*, 136. [[CrossRef](#)]
56. Gopal, A.; Kant, V.; Gopalakrishnan, A.; Tandan, S.K.; Kumar, D. Chitosan-based copper nanocomposite accelerates healing in excision wound model in rats. *Eur. J. Pharmacol.* **2014**, *731*, 8–19. [[CrossRef](#)]
57. Gushiken, L.F.S.; Beserra, F.P.; Hussni, M.F.; Gonzaga, M.T.; Ribeiro, V.P.; De Souza, P.F.; Campos, J.C.L.; Massaro, T.N.C.; Hussni, C.A.; Takahira, R.K. Beta-caryophyllene as an antioxidant, anti-inflammatory and re-epithelialization activities in a rat skin wound excision model. *Oxidative Med. Cell. Longev.* **2022**, 9004014. [[CrossRef](#)] [[PubMed](#)]
58. Bancroft, J.D. *Histochemical Techniques*; Butterworth-Heinemann: Oxford, UK, 2013.

59. Seif, M.; Deabes, M.; El-Askary, A.; El-Kott, A.F.; Albadrani, G.M.; Seif, A.; Wang, Z. Ephedra sinica mitigates hepatic oxidative stress and inflammation via suppressing the tlr4/myd88/nf- $\kappa$ b pathway in fipronil-treated rats. *Environ. Sci. Pollut. Res.* **2021**, *28*, 62943–62958. [[CrossRef](#)]
60. Asawa, Y.; Yoshimori, A.; Bajorath, J.; Nakamura, H. Prediction of an mmp-1 inhibitor activity cliff using the sar matrix approach and its experimental validation. *Sci. Rep.* **2020**, *10*, 14710. [[CrossRef](#)]
61. Pedretti, A.; Villa, L.; Vistoli, G. Vega—an open platform to develop chemo-bio-informatics applications, using plug-in architecture and script programming. *J. Comput.-Aided Mol. Des.* **2004**, *18*, 167–173. [[CrossRef](#)]
62. Trott, O.; Olson, A. Software news and update autodock vina: Improving the speed and accuracy of docking with a new scoring function, efficient optimization, and multithreading. *J. Comput. Chem.* **2010**, *31*, 455–461.
63. Petrescu, I.; Lamotte-Brasseur, J.; Chessa, J.-P.; Ntarima, P.; Claeysens, M.; Devreese, B.; Marino, G.; Gerday, C. Xylanase from the psychrophilic yeast *Cryptococcus adeliae*. *Extremophiles* **2000**, *4*, 137–144. [[CrossRef](#)] [[PubMed](#)]
64. Tantawy, M.A.; Sroor, F.M.; Mohamed, M.F.; El-Naggar, M.E.; Saleh, F.M.; Hassaneen, H.M.; Abdelhamid, I.A. Molecular docking study, cytotoxicity, cell cycle arrest and apoptotic induction of novel chalcones incorporating thiadiazolyl isoquinoline in cervical cancer. *Anti-Cancer Agents Med. Chem. (Former. Curr. Med. Chem.-Anti-Cancer Agents)* **2020**, *20*, 70–83. [[CrossRef](#)] [[PubMed](#)]
65. Daina, A.; Michielin, O.; Zoete, V. Swissadme: A free web tool to evaluate pharmacokinetics, drug-likeness and medicinal chemistry friendliness of small molecules. *Sci. Rep.* **2017**, *7*, 42717. [[CrossRef](#)]
66. Xiong, G.; Wu, Z.; Yi, J.; Fu, L.; Yang, Z.; Hsieh, C.; Yin, M.; Zeng, X.; Wu, C.; Lu, A. Admetlab 2.0: An integrated online platform for accurate and comprehensive predictions of admet properties. *Nucleic Acids Res.* **2021**, *49*, W5–W14. [[CrossRef](#)] [[PubMed](#)]

**Disclaimer/Publisher's Note:** The statements, opinions and data contained in all publications are solely those of the individual author(s) and contributor(s) and not of MDPI and/or the editor(s). MDPI and/or the editor(s) disclaim responsibility for any injury to people or property resulting from any ideas, methods, instructions or products referred to in the content.